Dynamics of component carbon fluxes in a semi-arid *Acacia* woodland, central Australia

James Cleverly,[1] Nicolas Boulain,[1] Randol Villalobos-Vega,[1] Nicole Grant,[1] Ralph Faux,[1] Cameron Wood,[2] Peter G. Cook,[2,3] Qiang Yu,[1] Andrea Leigh,[1] and Derek Eamus [1,4]

Received 5 March 2013; revised 22 July 2013; accepted 25 July 2013; published 29 August 2013.

[1] Vast areas in the interior of Australia are exposed to regular but infrequent periods of heavy rainfall, interspersed with long periods at high temperatures, but little is known of the carbon budget of these remote areas or how they respond to extreme precipitation. In this study, we applied three methods to partition net ecosystem photosynthesis into gross primary production (GPP) and ecosystem respiration (R_e) during two years of contrasting rainfall. The first year was wet (>250 mm above average rainfall), while little precipitation fell during the second year (>100 mm below average). During the first year of study, rates of GPP were large (793 g C m^{-2} yr^{-1}) in this semi-arid Mulga (*Acacia aneura*) and grass savanna due to complementary photosynthetic responses by the canopy and C_4 understorey to cycles of heavy rainfall. Patterns in GPP during the summer and autumn matched those in leaf area index (LAI), photosynthetic activity, and autotrophic respiration. During the dry year, small but positive photosynthetic uptake by Mulga contributed to the neutral carbon budget (GPP / $R_e = 1.06 \pm 0.03$). Small rates of photosynthesis by evergreen Mulga when dry were supported by storage of soil moisture above a relatively shallow hardpan. Little soil organic matter (1.1%) was available to support heterotrophic respiration (R_h) without input of fresh substrate. The two largest sources of R_e in this study were autotrophic respiration by the seasonal understorey and R_h through decomposition of fresh organic matter supplied by the senescent understorey.

Citation: Cleverly, J., N. Boulain, R. Villalobos-Vega, N. Grant, R. Faux, C. Wood, P. G. Cook, Q. Yu, A. Leigh, and D. Eamus (2013), Dynamics of component carbon fluxes in a semi-arid *Acacia* woodland, central Australia, *J. Geophys. Res. Biogeosci.*, *118*, 1168–1185, doi:10.1002/jgrg.20101.

1. Introduction

[2] Arid and semi-arid regions cover an estimated 20% of the globe [*Prentice et al.*, 2001; *Liu et al.*, 2012], exerting influence on global climate and atmospheric carbon dynamics. Semi-arid ecosystems experience extremes in temperature, moisture availability, and sunlight, which can act together to generate large photosynthetic and respiratory carbon fluxes [*Huxman et al.*, 2004a; *Baldocchi*, 2008; *Wohlfahrt et al.*, 2008; *Yan et al.*, 2011]. In Australia, the driest permanently inhabited continent on Earth, 70% of the land area is arid or semi-arid where potential evapotranspiration rates are high relative to precipitation [*Warner*, 2004; *Eamus et al.*, 2006]. Owing to the remoteness of much of Australia's interior, little is known about carbon dynamics in its semi-arid regions. The overall objective of this study was to describe ecosystem photosynthetic and respiratory carbon fluxes in central Australia by identifying responses of ecosystem component carbon fluxes to variations in meteorology, soil conditions, leaf physiology, and community composition of the active vegetation.

[3] Global flux networks measure the net ecosystem exchange (NEE) of CO_2 between ecosystems and the atmosphere, wherein partitioning of NEE elucidates changes in ecosystem respiration (R_e) and gross primary production (GPP) as ecosystems respond to a variety of stressors and disturbances [*Baldocchi*, 2008]. Net ecosystem photosynthesis (NEP) is analogous to net photosynthetic assimilation (A) in leaves, is positive during net carbon uptake (i.e., a carbon sink), and is the inverse of NEE [*Wohlfahrt et al.*, 2005]:

$$-\mathrm{NEE} = \mathrm{NEP} = \mathrm{GPP} - R_e, \quad (1)$$

where R_e is the sum of autotrophic and heterotrophic respiration (R_a and R_h, respectively) and includes carbon losses due to geophysical processes (e.g., photodegradation). In practice, R_e is estimated when GPP is known to be 0, either at

[1]School of the Environment, University of Technology Sydney, Broadway, New South Wales, Australia.
[2]National Centre for Groundwater Research and Training, School of Environment, Flinders University, Adelaide, South Australia, Australia.
[3]Water for a Healthy Country National Research Flagship, Division of Land and Water, Commonwealth Scientific and Industrial Research Organization, Adelaide, South Australia, Australia.
[4]National Centre for Groundwater Research and Training, University of Technology Sydney, Broadway, New South Wales, Australia.

Corresponding author: J. Cleverly, School of the Environment, University of Technology Sydney, PO Box 123, Broadway, NSW 2007, Australia. (James.Cleverly@UTS.edu.au)

2169-8953/13/10.1002/jgrg.20101

night [*Reichstein et al*., 2005] or at the intercept of a photosynthetic light response function (LRF) [*Lasslop et al*., 2010; *Lasslop et al*., 2012]. When extrapolating from nocturnal to daytime temperatures, overestimation of R_e can be avoided by estimating ecosystem "dark" respiration (R_d) from the intercept of LRFs [*Wohlfahrt et al*., 2005; *Baldocchi*, 2008; *Lasslop et al*., 2010]. In semi-arid regions, NEP increases with light as expected up to about half of full sunlight, but then it is not unusual for NEP to become negative such that R_e in full sunlight may exceed the value of ecosystem R_d [*Scott et al*., 2010]. Thus, R_e was estimated in our study during each of three time periods: night, daytime when solar irradiance (E_s) was smaller than half of full sunlight, and daytime in high light.

[4] In arid and semi-arid ecosystems, R_e and GPP are dependent upon delivery of rainfall and associated increases in soil wetness [*Eamus*, 2003; *Baldocchi*, 2008; *Yan et al*., 2011], although the seasonality of weather systems that deliver precipitation influences the strength and occurrence of photosynthetic and respiratory responses [*Reynolds et al*., 1999; *Hastings et al*., 2005]. Precipitation falling in winter storms is typically delivered by large frontal systems that can persist over hours or even days and generate low intensity rainfall of wide spatial extent, thereby recharging soil moisture. Both R_e and GPP can be enhanced by storage of winter moisture, consequentially having a much greater effect on global carbon cycling than otherwise expected [*Wohlfahrt et al*., 2008]. In contrast to winter storms, summer convective storms develop in response to local surface heating, creating intense, short-lived, and spatially varied rainfall when sufficient atmospheric moisture is present [*Berry et al*., 2011]. Unpredictability in timing and intensity of summer precipitation restricts ecosystem GPP responses to large or, more importantly, cyclically recurring precipitation pulses that have an effect on soil moisture [*Ma et al*., 2012].

[5] Because of the short-lived and unpredictable nature of summer storms, responses of GPP or R_e to summer rainfall pulses depend upon receipt of adequate rainfall to evoke a response (i.e., pulse-threshold-response) [*Schwinning and Sala*, 2004]. The response of R_e to a pulse of rainfall typically occurs within a day when storm size is larger than a threshold (typically between 5 and 13 mm) [*Huxman et al*., 2004b; *Baldocchi*, 2008; *Liu et al*., 2012]. During long periods between precipitation pulses, soil microbial activity is limited by low soil moisture (θ), thus litter tends to accumulate beneath C_3 woody vegetation into fertile islands [*Cable et al*., 2012]. Fertile islands contain labile sources of soil organic matter that are ready to support large pulses of R_e upon priming by moisture [*Cable et al*., 2012; *Ma et al*., 2012]. When a large rainfall pulse then occurs, the response of R_e precedes the response of GPP, which can result in a switch in sign of NEE from negative before rainfall, to positive immediately afterward, and sometimes back to negative [*Huxman et al*., 2004a; *Luo et al*., 2007; *Wohlfahrt et al*., 2008]. An understanding of the conditions under which component carbon fluxes are enhanced following precipitation pulses can better inform land surface models and improve simulations of carbon dynamics, which universally underestimate R_e and overestimate R_a in semi-arid regions [*Mitchell et al*., 2011]. Consequently, the first aim of this study was to evaluate the functional responses of component carbon fluxes to potential meteorological and physical drivers.

[6] Rainfall is a primary driver for carbon and water fluxes in all semi-arid areas, but the patterns are especially apparent in central and northern Australia because of the large interannual variability in rainfall that is skewed toward infrequent, very wet years [*Van Etten*, 2009; *Bowman et al*., 2010; *Morton et al*., 2011; *Papalexiou and Koutsoyiannis*, 2013]. Storms can be formed in these regions by two mechanisms: the monsoon depression can bring moisture during the summer, while synoptic frontal systems can bring large cold fronts across the continent year-round [*Zhang*, 2010]. However, in central Australia, either storm system is unlikely to be strong in any given year [*Berry et al*., 2011]. It is during infrequent wet years that central Australia is distinguished by extreme precipitation. In contrast to other global semi-arid regions where frontal rainfall is restricted to winter, interactions between continental cold fronts and the monsoon depression can augment summer rainfall in central Australia, thereby generating storms with the persistence and spatial extent of winter storms but delivering higher intensity rainfall than is generated by convection storms alone [*Kong and Zhao*, 2010].

[7] Differences in photosynthetic capacity and leaf area index (LAI) between C_3 and C_4 vegetation dictate the timing and size of ecosystem photosynthetic and respiratory responses to precipitation pulses [*Hattersley*, 1983; *Whitley et al*., 2011; *Barron-Gafford et al*., 2012]. For example, woody vegetation is known to maintain photosynthesis over a wide range of temperatures and soil moistures, while the C_4 grass layer is likely to contribute most of the annual GPP but only during the wet season [*Hutley et al*., 2005; *O'Grady et al*., 2009; *Whitley et al*., 2011; *Barron-Gafford et al*., 2012]. The vegetation over much of semi-arid, central Australia contains both C_3 and C_4 vegetation in a mosaic of two types of savanna, a biome containing an almost continuous grassy understorey and a discontinuous tree layer [*Eamus and Prior*, 2001]: (1) Mulga (*Acacia* spp.) woodland and (2) low, open eucalypt savanna with extensive Spinifex grass (*Triodia* spp.) and sparse *Corymbia* and *Eucalyptus* trees [*Hutley et al*., 2005; *Eamus et al*., 2006; *O'Grady et al*., 2009; *Eamus et al*., 2013]. The second aim of this work was to investigate the relationships between leaf function (A, R_a) and ecosystem carbon fluxes (NEP, GPP, and R_e) as they respond to seasonality, light, humidity, and soil moisture content.

[8] This study will focus on a Mulga woodland savanna during a 2 year period that was characterized by a juxtaposition of extremely wet and dry years. We tested three research hypotheses in this study. First, the large, cyclically recurring storms of central Australia were hypothesized to strongly enhance GPP by providing substantial soil moisture and reduced vapor pressure deficit interspersed with periods of clear skies and full sunlight. Consequently, GPP was expected to be larger than R_e in the wet year (i.e., carbon sink) but smaller than R_e in the dry year (i.e., carbon source), which is generally observed in other semi-arid regions [*Huxman et al*., 2004a; *Baldocchi*, 2008; *Wohlfahrt et al*., 2008; *Yan et al*., 2011]. Third, we hypothesized that ecosystem photosynthesis would reflect the seasonal activity of C_4 vegetation in the summer and C_3 vegetation during the remainder of the year.

2. Material and Methods

2.1. Site Description

[9] This study site is part of the Terrestrial Ecosystem Research Network's (TERN) OzFlux and Australian Supersite Network (ASN) programs and is located on Pine Hill cattle station near Ti Tree NT, central Australia (22.28° S, 133.25°E, 549 m asl). At the nearby Bureau of Meteorology station on the Territory Grape Farm (BOM TGF), mean and median annual rainfall has been 318.3 and 297.8 mm, respectively, since recording began in 1987 (http://www.bom.gov.au/). Of the annual median rainfall, 72% falls during the summer months (DJF) and 86% falls during monsoon season (Nov–Apr), placing the site just inside the Australian Monsoon Tropics [*Bowman et al*., 2010; *Hutley et al*., 2011]. Air temperature at the site can range from a low of −4°C (11 August 1994) to a high of 46°C (5 January 1994) (http://www.bom.gov.au/), although mean minimal and maximal temperatures are in the range of 5°C and 22.6° C in July to 22°C and 37.5°C in January.

[10] The soil is a heavily weathered red kandosol, which is typical of large portions of semi-arid Australia and has a high potential for drainage [*Schmidt et al*., 2010; *Morton et al*., 2011]. The soil characteristics of this site have been described in *Eamus et al*. [2013] and are summarized here. The surface bulk density is 1.69 ± 0.02 g cm^{-3}. Soil texture is a sandy loam (74/11/15% sand/silt/clay), and depth to groundwater is 49 m. Soil organic matter content (g) in 100 g of soil is equal to 1.1% at the surface and declines to 0.7 ± 0.1% at 1 m deep. The minimal soil organic matter content (0.5%) was observed where hardpan was encountered. Bare soil patches are likely surface expressions of the hardpan. Hardpan formation in the top meter, and possibly deeper, is commonly observed with this type of soil [*Morton et al*., 2011]. Variability in the depth of the hardpan implies that root development, near-surface storage of soil moisture, and infiltration are spatially heterogeneous in this flat (slope = 0.2%) landscape.

[11] This study was located in a Mulga savanna woodland at the southern end of the North Australian tropical transect [*Hutley et al*., 2011]. Mulga woodlands are widespread across Australia, covering 20–25% of the land surface area [*Nicholas et al*., 2011]. This site contains three varieties of Mulga and their hybrids, all of which form symbioses with nitrogen fixing cyanobacteria: *Acacia aneura* var. *aneura*, *A. aneura* var. *intermedia*, and *A. aneura* var. *tenuis*. The woodland canopy is 6.5 m tall and forms an incomplete cover with a basal area of 8 m^2 ha^{-1}. A patch of Spinifex grass (*Triodia* sp.), which crosses sharp ecotones to form a mosaic with Mulga [*Nicholas et al*., 2011], is located in a small gap (ca. 150 m^2) within the measurement footprint of the eddy covariance system. The dominant understorey forbs and shrubs are distributed sparsely throughout the measurement fetch and include *Psydrax latifolia*, *Eremophila gilesii*, *E. latrobei* ssp *glabra* (Crimson turkey bush), *Sida and Abutilon* spp., *and Solanum ellipticum* (Potato bush). The dominant grasses form a nearly complete cover when conditions permit and include perennials *Thyridolepis mitchelliana* (Window mulga-grass), *Eragrostis eriopoda* (Naked woolybutt grass), and annual *Eriachne pulchella* ssp *pulchella* (Pretty wanderrie). Like the forbs and shrubs, mulga-grass uses the C_3 photosynthetic pathway [*Christie*, 1975]. The remaining grasses use the C_4 photosynthetic pathway [*Hattersley*, 1983; *Simon and Alfonso*, 2011]. Growth and photosynthesis in the understorey are moisture dependent, and the C_4 component is more likely to be active in the summer than in other seasons [*Cable et al*., 2012]. Below the understorey, cryptobiotic crusts form a widespread ground cover that may contribute to rapid carbon turnover [*Jameson*, 2012] in response to small precipitation events [*Schwinning and Sala*, 2004].

2.2. Eddy Covariance, Meteorology, and Soil Measurements

[12] An eddy covariance system was employed to measure fluxes of carbon, water vapor, and energy. Beginning 2 September 2010, measurements of three-dimensional wind speed (CSAT3 sonic anemometer, Campbell Scientific Inc., Logan, UT, USA), virtual temperature (CSAT3), moisture density in air (Licor LI7500, LiCor Biosciences, Lincoln, NE, USA), and CO_2 density in air (LI7500) were sampled at a frequency of 10 Hz. Covariances were computed every 30 min to generate fluxes following standard OzFlux QA/QC and corrections procedures, which include but are not limited to [*Cleverly*, 2011; *Eamus et al*., 2013]: outlier and spike removal, co-ordinate rotation, frequency attenuation correction, conversion of virtual heat flux to sensible heat flux, and the WPL correction [*Wesely*, 1970; *Webb et al*., 1980; *Schotanus et al*., 1983; *Campbell Scientific Inc*., 2004; *Massman and Clement*, 2004]. The eddy covariance system was mounted to a tower (Nally Instrument Towers, Adelaide, SA, Australia) at a height of 11.7 m and oriented toward the southeast, centered on the historically predominant wind direction ranging from easterlies to southerlies [*Chen et al*., 1991]. Energy balance closure, as determined by the ratio of daily total outgoing radiation and energy fluxes to total daily incoming radiation and energy fluxes, was 0.97 [*Eamus et al*., 2013].

[13] A threshold for friction coefficient (u*) filtering was identified to be 0.25 m s^{-1} from the relationship between NEE and u*. To do this, values of NEE were grouped into u* classes of 0.05 m s^{-1} and plotted against average NEE in that class. When applying the u* filter, 56% of NEE measurements were discarded when u* was smaller than the threshold. Failure to apply the u* filter results in underestimation of nocturnal fluxes in the presence of drainage flow or when turbulence within and above the canopy are decoupled [*Aubinet*, 2008; *van Gorsel et al*., 2008; *van Gorsel et al*., 2011; *Oliveira et al*., 2013]. However, wind measured beneath the top of the canopy was negligible whenever u* was below the threshold (data not shown), thus implying that (1) within and above canopy conditions were closely coupled, (2) cold air drainage was unlikely, and (3) large ejections during turbulent periods that follow nonturbulent conditions reflect storage fluxes. The effect of the u* filter on estimation of nocturnal respiration was evaluated by comparing filtered and nonfiltered fluxes (section 2.5.2).

[14] Auxiliary observations of solar irradiance (E_s), soil moisture content (θ), soil temperature (T_s), vapor pressure deficit (D), and rainfall were collected to identify relationships between meteorology and carbon fluxes. Incident E_s was observed from a four-component radiometer that was positioned at a height of 12.6 m (CNR1, Kipp and Zonen, Delft, The Netherlends). D was determined as the difference

between atmospheric vapor pressure (kPa) and saturation vapor pressure at air temperature (HMP45C, Vaisala, Helsinki, Finland) at a height of 11.7 m. Onsite rainfall (CS7000, Hydrologic services, Warwick, NSW, Australia) was measured at a height of 2.5 m from the center of a 10 × 15 m clearing within the footprint of the tower. Surface θ was measured using soil water content reflectometers (CS616, Campbell Scientific Inc., Logan, UT) that were inserted horizontally with the upper and lower rods at 0.025 and 0.057 m deep, respectively. Surface T_s was observed using averaging soil thermocouples at depths of 2 and 6 cm. Temperature-corrected CS616 output was compared to gravimetric measurements from intact soil cores to empirically correct observed soil moisture to actual soil moisture (as described in *Eamus et al*. [2013]). Profile measurements of θ to a depth to 100 cm were collected using time domain reflectometry (CS605 and TDR100, Campbell Scientific Australia, QLD, Australia). To represent on-site variability in soil measurements, sensors were placed in microhabitats identified as bare soil, beneath Mulga canopies, and beneath understorey vegetation.

[15] To obtain a full, 2 year record of NEP, gaps that were introduced during QA/QC procedures were filled using a self-organizing linear output (SOLO) model. The SOLO model is a type of artificial neural network (ANN) that was trained on a self-organizing feature map (SOFM) of interrelationships between regressors: seven in this case [*Eamus et al*., 2013]. These regressors were determined through stepwise procedures and were: soil heat flux including heat storage above the sensors, net radiation, T_s, θ, atmospheric specific humidity, air temperature, and D [*Hsu et al*., 2002; *Abramowitz et al*., 2006; *Eamus et al*., 2013]. The combination of SOLO and SOFM procedures is the ANN analogue of multivariate analysis of covariance (MANCOVA), which results in low model error estimates (as small as 8 mmol m^{-2} day^{-1} RMSE [*Eamus et al*., 2013]).

2.3. Leaf Area Index, Leaf Physiology, and Autotrophic Respiration

[16] Leaf area index of the canopy and understorey was measured optically using the digital photography method [*Macfarlane et al*., 2007] as described in *Eamus et al*. [2013]. In short, 100 m transects were established within the tower fetch in cardinal quarter-directions: i.e., east, southeast, south, etc. Photographs were taken using a Canon DSLR camera fitted with a lens of short focal length (18 mm). The camera was oriented to 0° nadir (viewing upward) and 57.5° to the vertical (viewing downward) for canopy and understorey LAI, respectively.

[17] Satellite remote sensing was used to estimate LAI during the periods between site visits. Total site LAI was estimated using the MODIS product MOD15A2, which is provided as an 8 day composite average and matches total LAI measured photographically at this site [*Eamus et al*., 2013]. A spline function was fit to MODIS LAI to interpolate daily total LAI. Spline functions were also fit to the temporal sequence of canopy and understorey LAI observations to construct interpolated time series of proportional contributions to total LAI. A lower limit of 0.1 was set for the canopy to avoid unrealistic estimates of LAI in evergreen Mulga.

[18] Leaf gas exchange measurements were collected from Mulga and representative understorey leaves. Leaf photosynthetic LRFs to incident photosynthetically active radiation (PAR) were collected with a Licor 6400 (Licor LI6400XT, Li-Cor Biosciences, Lincoln, NE) on clusters of leaves of terminal branches during two measurement campaigns. To obtain LRFs, an external light source was used to increase PAR systematically from dark to a maximum of 3000 μmol m^{-2} s^{-1} after dark adapting in the cuvette for a minimum of 5 min to 10 min before the first measurement. LRFs on Mulga leaves were measured in the morning and at midday in December 2010 to identify A in full sunlight (A^{sat}) early in the growing season before NEP became large.

[19] The y-intercept where the LRF goes to PAR of 0 was used as an estimate of leaf dark respiration (R_d [μmol m^{-2} s^{-1}]). Measurements on Mulga leaves were collected 30 March to 2 April 2011 between 7.00 and 14.00. LRFs were measured for understorey leaves 4–7 April 2011, also between 7.00 and 14.00. Measured values of R_d are sensitive to enhancement of carbon fluxes due to predarkening illumination (i.e., light enhanced dark respiration, LEDR) [*Atkin et al*., 1998; *Barbour et al*., 2007; *Barbour et al*., 2011]. While LEDR can cause overestimation of R_d for 50–100 min after darkening [*Atkin et al*., 1998; *Barbour et al*., 2007], the effect is minimal in low light (e.g., during the 7.00 measurements) [*Atkin et al*., 1998; *Barbour et al*., 2011] and during a short period ca. 5–10 min after darkening, which is when LEDR is compensated by inhibition of R_d in the light [*Atkin et al*., 1998]. Thus, overestimation of R_d due to LEDR was expected to be present but minimal in our study.

[20] Measurements of leaf-level R_d were scaled by LAI to estimate daily R_a. The diurnal course of R_d was integrated across the daily series of LRFs (7.00 to 14.00) to estimate total daily R_d. Daily fraction of R_a from each vegetation layer (i.e., understorey or canopy) was determined as the product of LAI and total R_d. Proportions of canopy and understorey LAI were extrapolated to the beginning of the eddy covariance time series by maintaining a constant proportionality with the first measurement date. The daily sum of canopy and understorey values of total R_d × LAI was taken to be an estimate of total ecosystem R_a.

2.4. Light Response Functions and Ecosystem Metabolism

[21] The rectangular hyperbolic light response function was chosen for its simplicity, common use in photosynthesis modeling, and previous demonstration of its applicability in eddy covariance carbon research [*Wohlfahrt et al*., 2005; *Lasslop et al*., 2010]:

$$NEP = \frac{\alpha\beta E_s}{\alpha E_s + \beta} + \gamma, \tag{2}$$

where α is the slope at low light and represents ecosystem quantum yield, β is maximum NEP (NEP^{max}) and is analogous to the maximum photosynthetic rate (A^{max}), and γ is the y-intercept where E_s is zero.

[22] Short-term analysis of ecosystem metabolism included 30 min observations of E_s and NEP, averaged over four 6 day periods: (1) springtime when the ecosystem was a carbon source (23–29 Nov 2010), (2) following an early summer rainfall event that resulted in the carbon balance switching from a source to a sink (10–16 Dec 2011), (3) at the end of a very wet summer (20–26 Feb 2011), and (4)

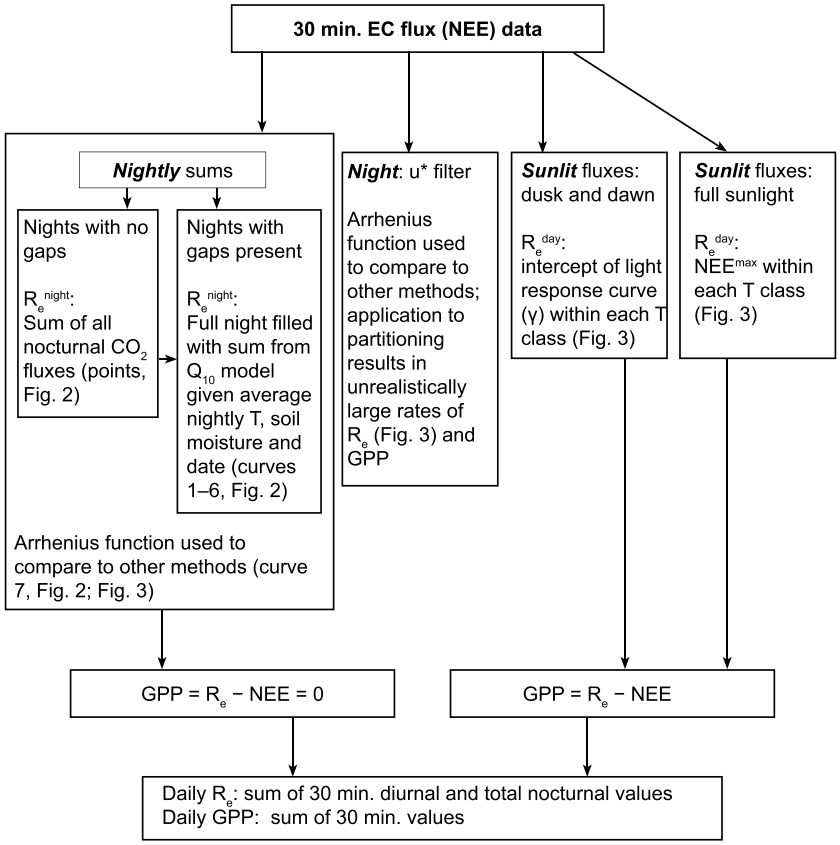

Figure 1. Schematic flow chart showing the methods for partitioning of carbon fluxes.

shortly after a large springtime rainfall event when the ecosystem was again a carbon source (25–31 Oct 2011). LRFs using EC flux data were created individually for morning (before 12:00 local standard time, LST) and afternoon measurements during these four periods.

2.5. Carbon Flux Partitioning

[23] Carbon fluxes were partitioned from NEE in two steps (Figure 1): first R_e was estimated, which was then used to estimate GPP in equation (1). R_e was estimated from the responses of NEE to temperature when GPP was assumed to be negligible. The manner in which GPP was assumed to be negligible depended on time of day and was grouped into three classes or "methods" (Figure 1): (1) night, (2) sunlit at dawn and dusk, and (3) under full sunlight periods (sections 2.5.1–2.5.4). T_s rather than T_a was chosen for functional response curves because (1) more than 60% of R_e originates from the soil [*Janssens et al*., 2001], (2) T_s was more representative of canopy and subcanopy T_a than measurements at 11.7 m (data not shown), and (3) use of a single temperature facilitates comparison of R_e rates among methods (section 2.5.5). Only flux data with gaps that were unfilled were used to estimate R_e to avoid the confounding effects of gap filling procedures, which are modeled in part on T_s, θ, and net radiation. All of the following subsections (2.5.1–2.5.6) refer to Figure 1.

2.5.1. Nocturnal Respiration: Nightly Sums

[24] Observations of NEE were accumulated over a full nocturnal period to avoid double accounting of carbon that is stored at one time of night and released at another. It was assumed that nocturnal GPP was 0; thus, R_e^{night} was assumed to be equal to total nocturnal NEE on nights without gaps in the flux data. These estimates of R_e^{night} include storage fluxes during intermittent turbulence and the morning transition from calm to turbulent conditions [*Aubinet*, 2008]. Sources of error in this approach include flux loss due to unaccounted horizontal losses of stored CO_2, which was minimal because of the flat topography (0.2% slope) and extensive fetch (> 10 km) at this site, and due to secondary uptake of respired CO_2 by early morning photosynthesis. Underestimation of R_e due to secondary uptake is more likely during the morning transition than during nocturnal episodes of intermittent turbulence. Thus, error of R_e^{night} that was estimated from nightly sums is expected to be proportional to the regression error term in thermal sensitivity functions (Figure 2).

[25] Thermal sensitivity functions were used to estimate values of R_e^{night} during nights when gaps were present in the data. To account for moisture limitation on R_e^{night}, nightly average θ was used to group nightly observations into three classes: low (3–5%), medium (5–10%), and high (10–22%). Thermal sensitivity curves were developed from R_e^{night} and T_s in each θ class on nights lacking data gaps. Within a θ class, thermal sensitivity was found to vary by measurement date ($\ln R_e^{night}$ ANCOVA; $F = 9.84$; $df = 5, 392$; $p < 0.0001$; Figure 2). Exponential (i.e., Q_{10}) functions were determined within each θ class and measurement period (Figure 2).

[26] Extrapolation of R_e^{night} to daytime temperatures for the purpose of comparing to estimates of R_e^{day} (sections 2.5.3–2.5.4) was done by fitting the Arrhenius function to

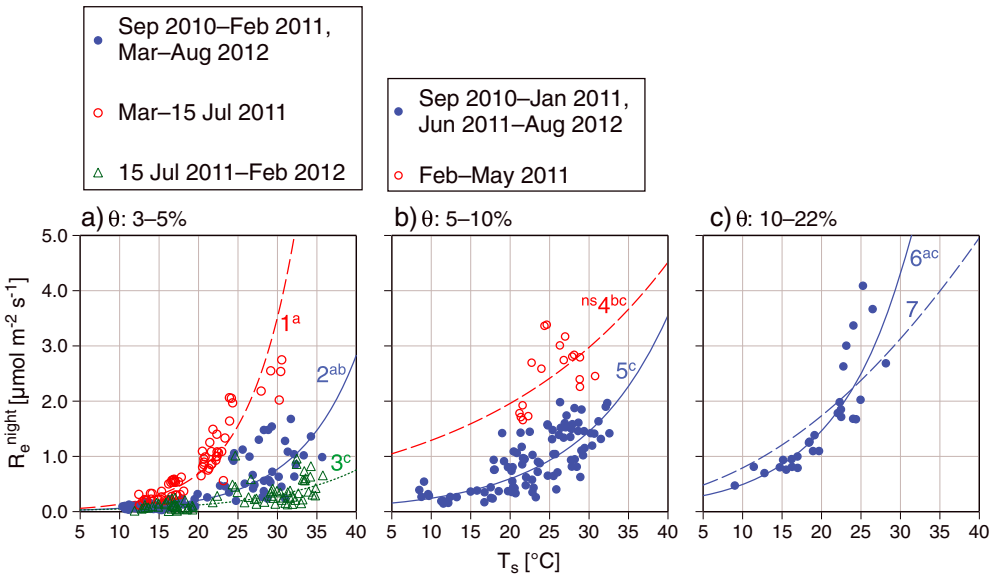

Figure 2. Average nocturnal ecosystem respiratory carbon flux (R_e^{night}) as a function of nightly average T_s. Data were categorized by date of measurement and within soil moisture (θ) classes of (a) 3–5%, (b) 5–10%, and (c) 10–22%. Curves 1–6: least squares regression curves representing exponential (Q_{10}) functions in which those marked with the same letter do not have a significantly different slope. ns: slope is not significantly different from zero. Curve 7: Arrhenius function fit to R_e^{night} in the wettest θ class.

R_e^{night} [*Lloyd and Taylor*, 1994]. Comparison between Q_{10} and Arrhenius functions is shown in the temperature sensitivity of wettest θ class (curves 6 and 7, respectively; Figure 2c). Because the Arrhenius function assumes that R_e is not limited by soil moisture availability [*Lloyd and Taylor*, 1994], extrapolation of R_e^{night} was performed using data from the wettest θ class. Because thermal sensitivity in the wettest θ class was not significantly different from Q_{10} in drier classes (Figure 2), the Arrhenius function was assumed to represent a general extrapolation of R_e to daytime temperature regimes.

2.5.2. Night: u* Filter

[27] Application of the u* filter to nocturnal fluxes resulted in a sample size of nights without gaps that was too small for nightly accumulation analysis. Consequently, thermal sensitivity was evaluated with 30 min fluxes rather than nightly total NEE (Figure 1). Extrapolation of u* filtered, nocturnal NEE fluxes to daytime temperature was performed using an Arrhenius function (section 2.5.1). In the presence of destorage fluxes during intermittent nocturnal turbulence, application of the u* filter results in overestimation of source fluxes [*Aubinet*, 2008]. Similarly, unrealistically large values of R_e were obtained from application of the u* filter in this study (Figure 3); thus, u* filtered fluxes were not used in carbon partitioning.

2.5.3. Sunlit Fluxes: Dusk and Dawn

[28] Photosynthetic LRFs that were constructed from NEP and E_s were used to estimate R_e^{day}. Daytime data (i.e., $E_s > 10$ W m^{-2}) were used to develop LRFs from the complete, 2 year data set. Observations of 30 min daytime NEP were grouped into 5°C T_s classes beginning at 6°C. Within a temperature class, a rectangular hyperbolic LRF was applied (nlinfit, Matlab) to obtain γ, an estimate of R_e^{day} at the point at which E_s and GPP decline to 0 [*Lasslop et al.*, 2010].

[29] During high-light conditions ($E_s > 500$ W m^{-2}) in semi-arid areas, midday carbon losses can be larger than γ [*Scott et al.*, 2010]. These large midday respiratory fluxes occur at higher temperatures than γ and are the result of

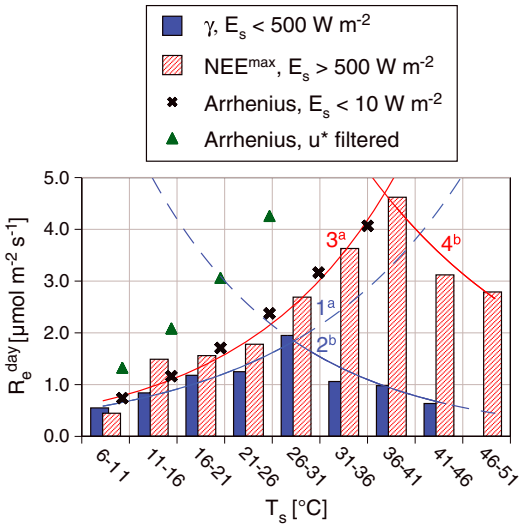

Figure 3. Daytime ecosystem respiration (R_e^{day}) as a function of soil temperature (T_s) class. Solid bars represent R_e^{day} estimated using the intercept of the light response curve (γ) and applied in low solar irradiance ($E_s < 500$ W m^{-2}). Striped bars represent the maximum observed daily net ecosystem exchange (NEE^{max}) in high light ($E_s > 500$ W m^{-2}). Crosses represent extrapolation of the nocturnal Arrhenius curve (curve 7, Figure 2) and triangles represent extrapolation of the nocturnal Arrhenius curve after application of the u* filter. Numbered lines: Q_{10} curves with the same letter do not have a significantly different slope.

Table 1. Summary of Leaf Gas Exchange Responses to Photosynthetically Active Radiation (PAR)[a]

Condition	Time	α	A^{sat}	A^{max}	R_d
Dry	Before 10.00	0.02139	1.89	3.16	−1.05
Dry	After 10.00	0.02139	0.69	2.11	−1.32
Wet	Before 10.00	0.02139	3.92	7.37	−2.37
Wet	After 10.00	0.02139	5.24	7.37	−1.05

[a]Condition: before (7 Dec 2010) and following (8 Dec 2010) overnight rainfall at the midpoint of a six-day rainfall event (53 mm); α: initial slope of the light response function; A^{sat}: net photosynthetic rate in full sunlight (2000 μmol m^{-2} s^{-1} PAR); A^{max}: maximum net photosynthetic rate; R_d: dark respiration (0 μmol m^{-2} s^{-1} PAR).

midday depression of photosynthesis. By assuming that depression of photosynthesis is least likely to confound LRF analysis in low light conditions, γ was taken to be an estimate of R_e^{day} when $E_s < 500$ W m^{-2} (i.e., dusk and dawn). Double exponential functions were fit to R_e^{day} at the midpoint of each T_s class to determine R_e^{day} from T_s in each 30 min period (Figure 3).

2.5.4. Sunlit Fluxes: Full Sunlight

[30] A special application of the LRF method was used to estimate R_e^{day} when $E_s > 500$ W m^{-2}. By identifying periods when A^{sat} can be assumed to equal zero, the LRF decomposes to the thermal sensitivity of NEE [*Lasslop et al.*, 2010; *Lasslop et al.*, 2012]. This is the first study to employ this application of LRFs to R_e^{day}. In our study, the 2 year maximal rate of NEE in high light (NEE^{max}) was identified in each of the 5°C T_s classes that were described in section 2.5.2. While not every incidence of positive NEE flux is associated with negligible GPP, the single value of NEE^{max} in each T_s class was assumed to occur when GPP = 0. This assumption is supported by previous observations of midday depression in Mulga leaves with consequential reduction of ET and stomatal conductance to zero [*Eamus et al.*, 2013]. Errors in estimation of R_e^{day} due to GPP > 0 would lead to under-estimation of both R_e and GPP.

2.5.5. Ecosystem Respiration: Method Comparison

[31] In summary, R_e was determined from Q_{10} thermal sensitivity functions at night and light response functions during the day (Figure 1):

$$R_e = \begin{cases} R_e^{night} = \sum NEE & \text{night : without gaps} \\ R_e^{night} = a\exp(bT_s)_{(\theta,date)} & \text{night : with gaps} \\ R_e^{day} = \gamma_{(T)} & \text{sunlit : } 10\ W\ m^{-2} < E_s < 500\ W\ m^{-2} \\ R_e^{day} = \gamma_{(T)}\big|_{GPP=0} = NEE_{(T)}^{max} & \text{sunlit : } E_s > 500\ W\ m^{-2}. \end{cases} \quad (3)$$

[32] All computational methods for estimating R_e were evaluated as a function of temperature (e.g., $\gamma_{(T)}$) with the exception of R_e^{night} on nights without gaps, which was totalled directly from measured NEE fluxes. Values of γ have been previously found to be in good agreement with combined measurements of nightly NEE and storage fluxes [*van Gorsel et al.*, 2009]. Extrapolation of R_e^{night} via the Arrhenius function when the u* filter was applied resulted in values of R_e^{day} that were much higher (2 to 3.5 times) than those of any other method. R_e estimated from each of these methods in the absence of the u* filter was in very close agreement at temperatures below their respective thermal optima (Figure 3), which implies that (1) the error implicit in estimated R_e from each method is of approximately the same magnitude and direction and (2) the assumptions of each method are more likely correct than violated.

[33] R_e^{day} increased exponentially with soil temperature (T_s) to a critical (optimum) temperature, which occurred at a higher

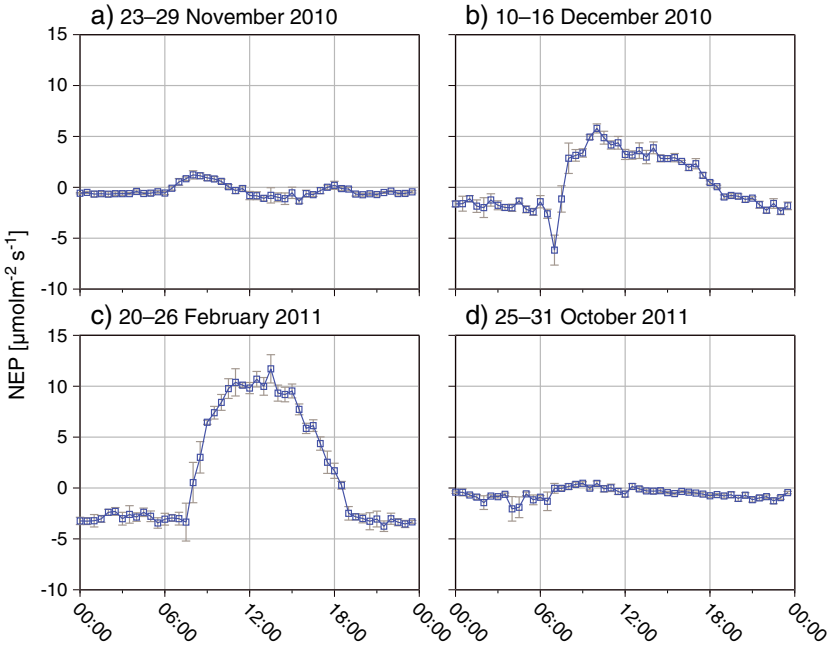

Figure 4. Average diel pattern of 30 min net ecosystem photosynthesis (NEP) ± se during four periods representing (a) the November carbon source period, (b) early heavy rainfall, (c) late heavy rainfall, and (d) at the end of extended drought.

Table 2. Summary of Annual Meteorology and Component Carbon Fluxes[a]

	2010–2011	2011–2012
n [days]	360	347
Rainfall [mm]	565.2	183.8
Rainfall (BOM) [mm]	542.6	258.4
T_s [°C]	24.3 ± 0.1	25.6 ± 0.1
D [kPa]	1.5 ± 0.01	2.0 ± 0.01
E_s [MJ m^{-2} day^{-1}]	22.0 ± 0.3	21.9 ± 0.3
θ [cm^3 (100 cm^3)$^{-1}$]	6.8 ± 0.04	4.7 ± 0.02
R_e^{day} (γ) [mol m^{-2} yr^{-1}]	6.3	5.8
R_e (Nocturnal) [mol m^{-2} yr^{-1}]	16.8	6.8
R_e^{day} (NEE^{max}) [mol m^{-2} yr^{-1}]	21.5	21.2
R_e [mol m^{-2} yr^{-1}]	44.6	33.9
NEP [mol m^{-2} yr^{-1}]	21.1	−0.3
GPP [mol m^{-2} yr^{-1}]	66.2	33.2
GPP / R_e	1.49 ± 0.03	1.06 ± 0.03

[a]Single values represent annual totals; Binomial values represent daily average ± standard error, se; T_s: soil temperature; D: vapor pressure deficit; E_s: solar irradiance; θ: % volumetric soil moisture content; R_e: ecosystem respiration; γ: estimate from intercept of the light response function; NEE^{max}: estimate from NEE^{max} method; NEP: net ecosystem photosynthesis; GPP: gross primary production.

temperature in high light ($E_s > 500$ W m^{-2}) than in low light ($\ln R_e^{day}$ ANCOVA; $F = 17.75$; $df = 3, 11$; $p = 0.002$; Figure 3). The difference in optimal temperature at dusk and dawn *versus* full sunlight is a result of the relatively cool morning and evening periods. Above the optimum temperature, R_e declined exponentially with increasing T_s for both daytime methods of calculation (Figure 3).

2.5.6. Gross Primary Production and Daily Totals

[34] Following determination of R_e, GPP was computed from the difference between R_e^{day} and NEE (Figure 1). By definition, R_e and NEE are equal in the nocturnal measurements; thus, GPP was set to 0 at night. Determination of 30 min GPP from the residual of R_e^{day} and NEE [e.g., *Reichstein et al.*, 2005] was chosen in favor of using LRFs to determine GPP [e.g., *Lasslop et al.*, 2010] because of (1) the relative importance of R_e in NEP at high light levels and (2) decoupling of LRF parameters and VPD (data not shown). Daily totals of GPP were determined from the sums of 30 min sunlit GPP and were computed from gap-filled NEE. Daily total R_e was determined from the sum of 30 min R_e^{day} and total R_e^{night}.

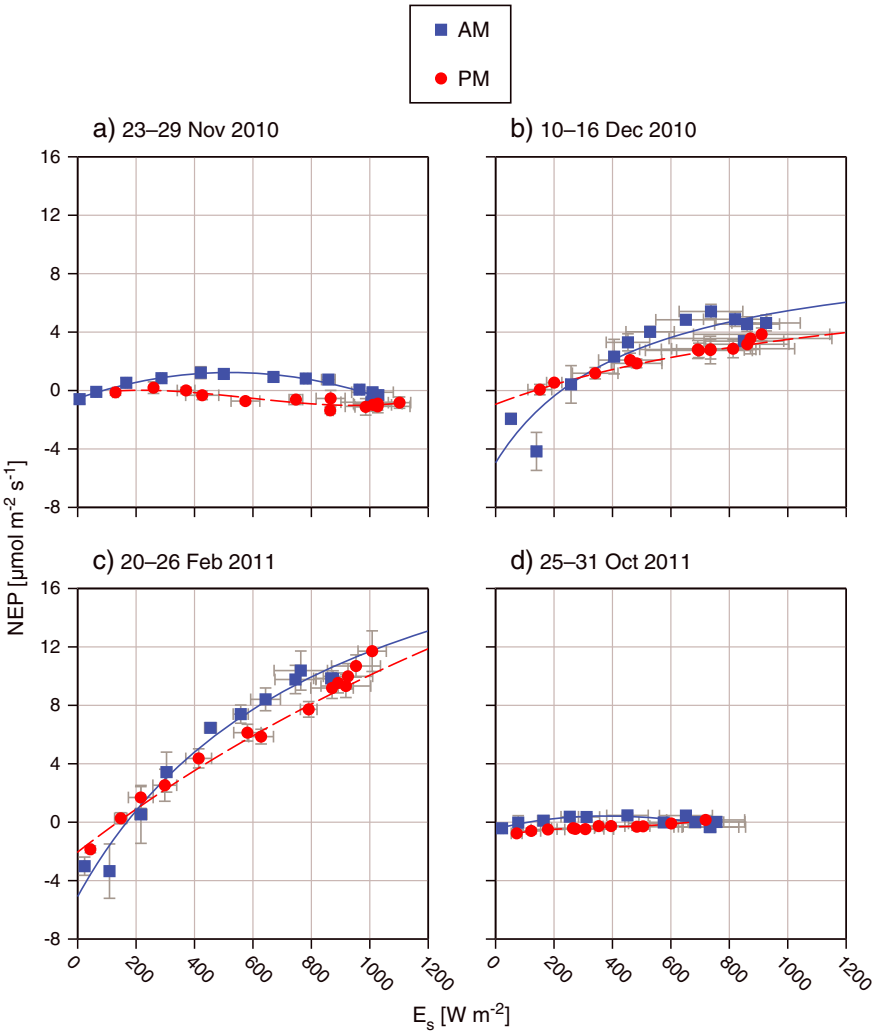

Figure 5. Ecosystem light response functions. Values represent 30 min average NEP ± se and E_s ± se. Curves in Figures 5a and 5d are third-order polynomials for illustrative purposes, while curves in Figures 5b and 5d are rectangular hyperbolic functions that were fit in the morning (AM; boxes and solid lines) and afternoon (PM; circles and dashed lines).

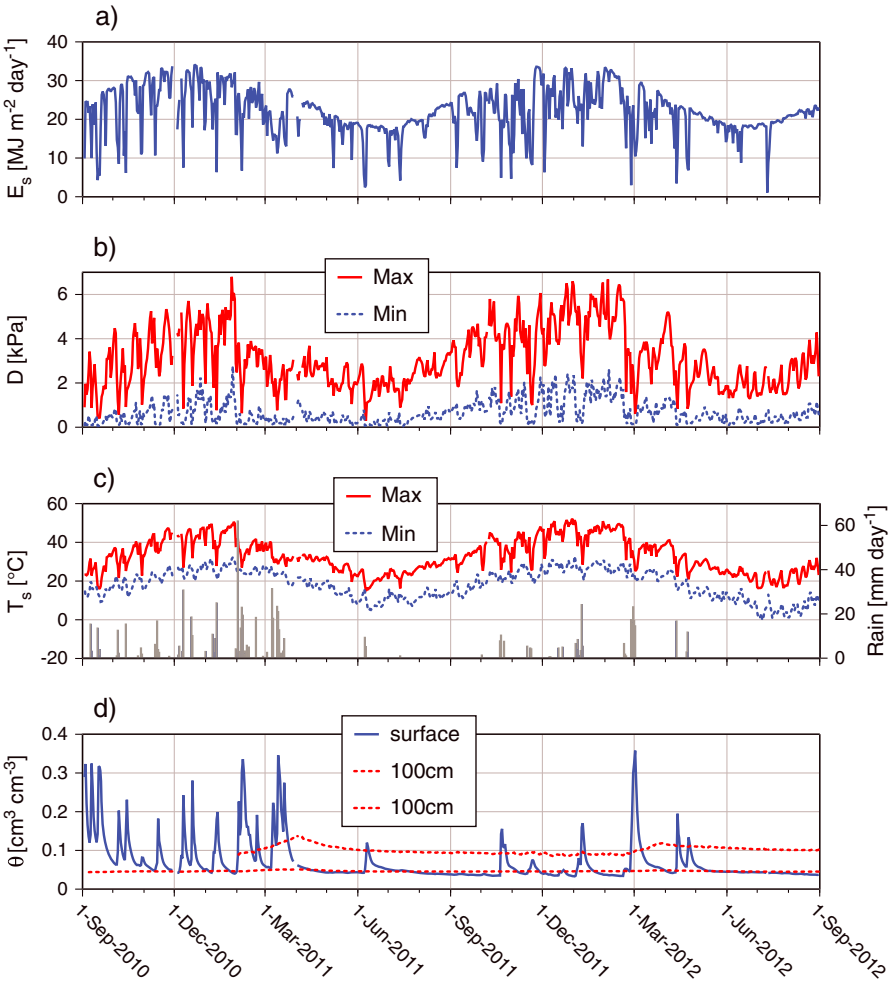

Figure 6. Seasonal time series of rainfall, E_s, vapor pressure deficit (D), T_s, and θ.

2.6. Data Analysis

[35] The temperature sensitivity of R_e^{night} (i.e., the slope of the relationship between R_e^{night} and T_s) was compared among θ classes and seasons using analysis of covariance (ANCOVA) between $\ln(R_e^{night})$ and T_s. In the event of rejecting the null hypothesis H_0: global slope $b = b_i = 0$ where the subscript i is the ith factor (observational period × θ class), *post-hoc* least significant differences (multiple comparisons) procedures were performed to test H_0: $b_i = b_j$ for all factorial pairs (i.e., H_0: slopes for each grouping are parallel). All statistical comparisons were performed using Type III sums of squares and a presumed critical $p = 0.05$ (Matlab 7.9.0 R2009b, The Mathworks, Natick, MA, USA). Double-exponential curves were applied (nlinfit) to R_e^{day} and T_s under each light level, and slopes were compared using ANCOVA as with R_e^{night}. Summary statistics of thermal sensitivities in R_e^{day} and R_e^{night} are presented in supporting information Table 1.

[36] The temporal dependence of R_e and GPP upon E_s, D, T_s, θ, and atmospheric pressure (P) was evaluated using power spectral and coherence analyses [*Cleverly et al.*, 2002]. These analyses were performed on 2^6 daily observations of total E_s, daily maximal and minimal D (D^{max} and D^{min}, respectively), maximal and minimal T_s (T_s^{max} and T_s^{min}, respectively), average θ, and average P. Three 64 day analysis windows covered the wet summer (30 Dec 2010 to 3 Mar 2011), winter 2011 (20 Jun to 22 Aug 2011), and the dry summer (30 Dec 2011 to 2 Mar 2012). Power spectral density (PSD) was computed for each time series using a fast Fourier transform (sptool, Matlab). Coherence between PSDs was computed using a Hanning window of length of 2^5 and window overlap of 2^4 (mscohere, Matlab). Coherence between PSDs is indicative of temporal squared correlation (0–1) between physical driving variables (e.g., θ) and R_e or GPP. Storm cycle period was identified from the peak frequency or frequencies in the coherence between E_s and θ to account for (1) periods of low pressure and cloudiness that do not produce rainfall and (2) phase shifting of θ to postrainfall exponential decay [*Eamus et al.*, 2013].

[37] Envelope analysis was used to evaluate the net and gross carbon flux limit within the observed range of E_s, D, T_s, and θ. In this example of an extreme value problem [*Coles*, 2001], observations of NEP, GPP, or R_e were blocked into meteorological classes, within which the maximal value was identified. A function was then applied that circumscribes the carbon flux maxima as a function of meteorological classes (e.g., see Figure 2 in *Whitley et al.* [2009]). Block maxima were determined in T_s classes of 5°C in width (e.g., 5–10, 50–55°C), D in classes of 0.65 kPa (e.g., 0–0.65,

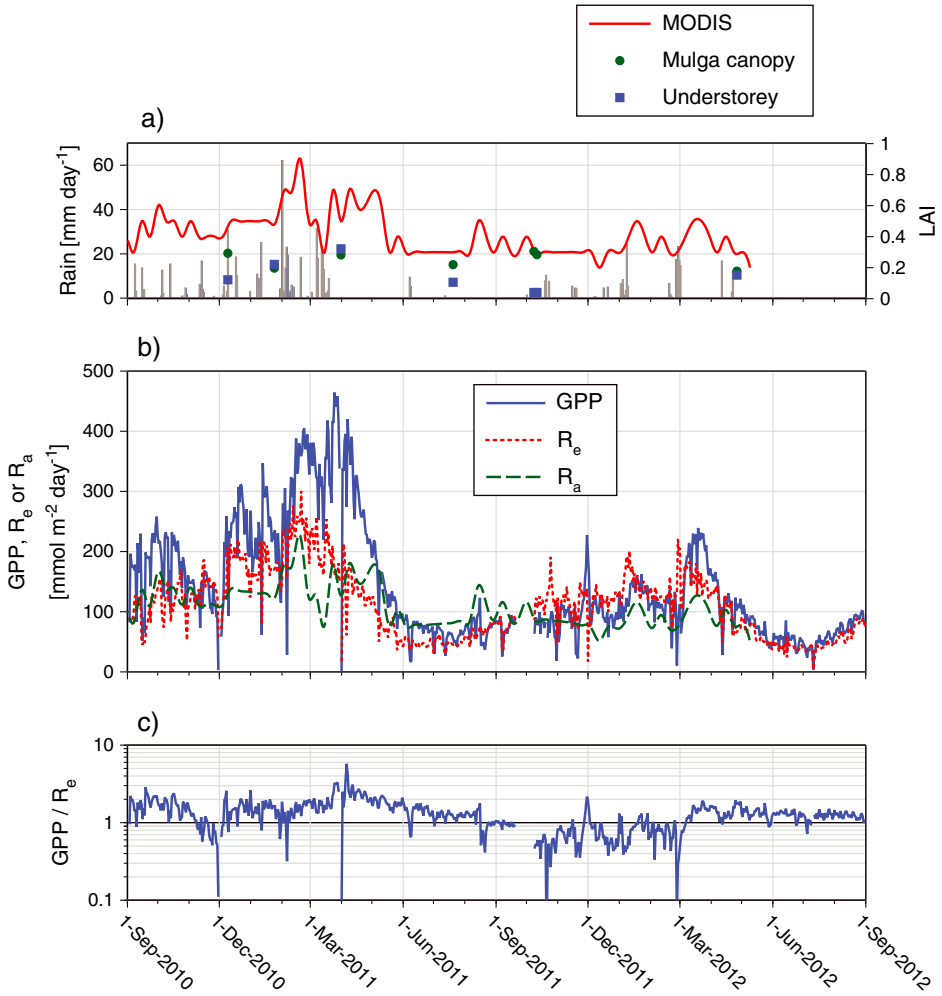

Figure 7. Seasonal patterns of MODIS LAI, daily rainfall, total gross primary production (GPP), ecosystem respiration (R_e), autotrophic respiration (R_a), and carbon balance (GPP / R_e). MODIS LAI was interpolated to daily values using a spline function.

5.2–5.85 kPa), and E_s in classes of 100 W m^{-2} (30 min observations) or 5 MJ m^{-2} day^{-1} (daily totals). All blocks were further divided into four θ classes: < 4%, 4–8%, 8–12%, and > 12% for daily average θ or < 5%, 5–11%, 11–17%, and > 17% in 30 min observations. The lowest E_s class (0–100 W m^{-2}) includes all nocturnal observations. For daily response functions, gap-filled data were used to avoid sample-size restrictions. In the 30 min observations, unfilled data sets were used to avoid autocorrelation with meteorological relationships that were incorporated during gap-filling procedures. Summary statistics of curves in the envelope analysis are presented in supporting information Table 2.

3. Results

3.1. Ecosystem and Leaf-Scale Photosynthesis

[38] Figure 4 shows the daily pattern of NEP in four contrasting periods across the study. Average T_s was 33.8 ± 0.4, 30.7 ± 0.4, 30.3 ± 0.2, and 27.8 ± 0.3°C during each period in Figures 4a–4d, respectively. The largest rate of NEP was observed in February 2011 (NEP > 10 µmol m^{-2} s^{-1}) and the largest negative extreme occurred during the early morning in December 2010 (NEP < −5 µmol m^{-2} s^{-1}; Figure 4). NEP was smallest during springtime (< 2 µmol m^{-2} s^{-1}), but positive photosynthetic activity was supported in the morning (Figures 4a and 4d). During midday, depression of NEP was common except during the late summer when NEP was largest (Figure 4). In February after two months of heavy rainfall, NEP peaked in the early afternoon rather than early morning (cf. Figures 4b and 4c). Periods of large nocturnal respiratory fluxes occurred during the morning transition (Figures 4b and 4c) and intermittently during the latter half of the night (Figure 4d).

[39] The ecosystem LRFs are shown in Figure 5. During the spring, NEP was positive in the morning under low light (Figures 5a and 5d). In the springtime, hysteresis in LRFs resulted in NEP that was smaller (i.e., more negative) when E_s > 500 W m^{-2} than when E_s was 0 (i.e., Figure 5a), which supports the assumption that GPP was negligible when NEE^{max} was measured in each of the nine T_s classes. Model parameters α and β were larger in the morning than in the afternoon, while γ was smaller in the morning (Figure 5). Ecosystem photosynthesis did not reach light saturation (i.e., the LRF did not reach a plateau) in February 2011. Values of γ ranged from −0.3 to −5 µmol m^{-2} s^{-1} across the four selected periods (Figure 5).

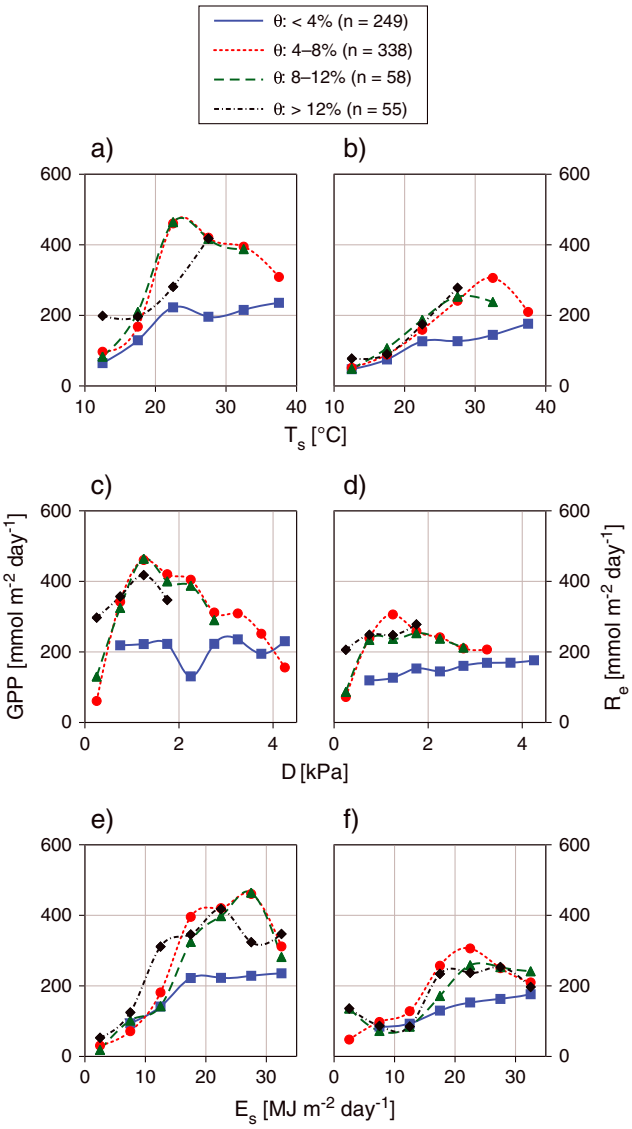

Figure 8. Parameter envelopes for GPP or R_e as functions of daily θ and T_s, D, or E_s. Splines were used for all curve fits. Points represent the maximal flux in a given θ × meteorology block. N = 700 days.

[40] Phyllode-scale A and R_d in Mulga showed large, short-term responses to rainfall (Table 1). Before rainfall resumed, small rates of A^{sat} during the morning declined to near zero by midday (Table 1), which further confirms the assumption that A and GPP are negligible at midday under some conditions. Just before rainfall, A^{sat} and R_d were small and then increased on the day following overnight rainfall. Before rainfall, R_d was slightly smaller in morning than at midday (Table 1). Conversely after rainfall, R_d was smaller at midday than in the morning (Table 1).

3.2. Meteorology and Soil Moisture

[41] More than three times the rainfall accumulated during the first year of study than during the second year (Table 2). Heavy precipitation fell in December 2010 through April 2011 (Figure 6). More than half of the dry year (2011–2012) rainfall (Table 2) fell in January and February 2012 (119.6 mm) (Figure 6). In 2011, April through September was a very dry period, receiving only 1.2 mm in total rainfall (Figure 6). Likewise, no precipitation was recorded during May through August 2012 (Figure 6). Total monthly rainfall was below average during 15 of 24 months, was 0 mm during 6 months, and was less than or equal to 1 mm in another 3 months. Meteorological drought, which is defined as three or more consecutive months of below average precipitation [*AMS*, 1997; *Dai*, 2011], was experienced three times: July–September 2011, November 2011 to February 2012, and May–August 2012 (Figure 6). The research site and nearby BOM TGF station did not receive substantially different rainfall amounts in the first year, but the difference between them was 74.6 mm in the second year (Table 2).

[42] Daily meteorology and soil water contents are shown in Figure 6. In the first year, mean daily surface θ was large (> 0.10 m^3 m^{-3}) and mean D small (Table 2), T_s exceeded 40°C in 4% of the total observations, and D exceeded 4 kPa during 4% of observations. During the second year, mean surface θ was small and mean D large (Table 2), T_s exceeded 40°C in 7% of observations, and D exceeded 4 kPa in 10% of observations. Neither average T_s nor average daily E_s was substantially different between years 1 and 2 (Table 2). Daily total E_s was largest in the summer during interstorm periods (e.g., 34.1 MJ m^{-2} day^{-1} on 21 Dec 2010) and was smallest during winter under deep cloud cover (e.g., 1.1 MJ m^{-2} day^{-1} on 11 Jul 2012), although E_s could be nearly as small during summer storms (e.g., 3.0 MJ m^{-2} day^{-1} on 27 Feb 2012; Figure 6).

[43] Storm and interstorm intervals resulted in large, rapid and cyclic shifts of E_s, D^{max}, T_s^{max}, and θ (Figure 6). Daily T_s^{max} and D^{max} increased through summer interstorm periods, reaching large values before dropping after the first major storm of the late summer or early autumn (Figure 6). Surface θ was regularly high (> 20%) in response to rainfall events in the first year, but only infrequently following rainfall in the second, drier year (Figure 6). Deep θ (100 cm) followed one of two patterns: (1) θ measured in one array was invariant and small (4.6 ± 0.005%) throughout the 2 year study period, or (2) θ measured in the other array was consistently larger (typically 10%) and increased slightly (2–4%) following series of storms, reaching a peak in the autumn (late Mar or early Apr) of both years of the study (Figure 6). This variability is the result of the spatial heterogeneity in the distribution of relatively shallow (typically 1 m) hardpans that prevent deep drainage of water.

3.3. Leaf Area Index, Respiration, and Gross Primary Production

[44] As with the meteorology, daily LAI and carbon fluxes were responsive to rainfall patterns (Figure 7). Canopy and understorey combined to result in a total LAI of 0.2–0.9 (Figure 7). Understorey LAI was low (but not 0 because of the presence of woody evergreen shrubs) in June and November 2011. R_a was smaller than R_e during the early autumn 2011 and larger than R_e at the end of that autumn (Figure 7). Fluctuations in R_a closely mirrored variation in LAI, from which R_a was scaled (Figure 7).

[45] Both R_e and GPP were larger in the first year than in the following year (Table 2). R_e^{night} was larger in the first year than the second (201 g C m^{-2} yr^{-1} and 82 g C m^{-2} yr^{-1}, respectively; Table 2). Total R_e was 25% larger during the first year than during the second year (535 g C m^{-2} yr^{-1}

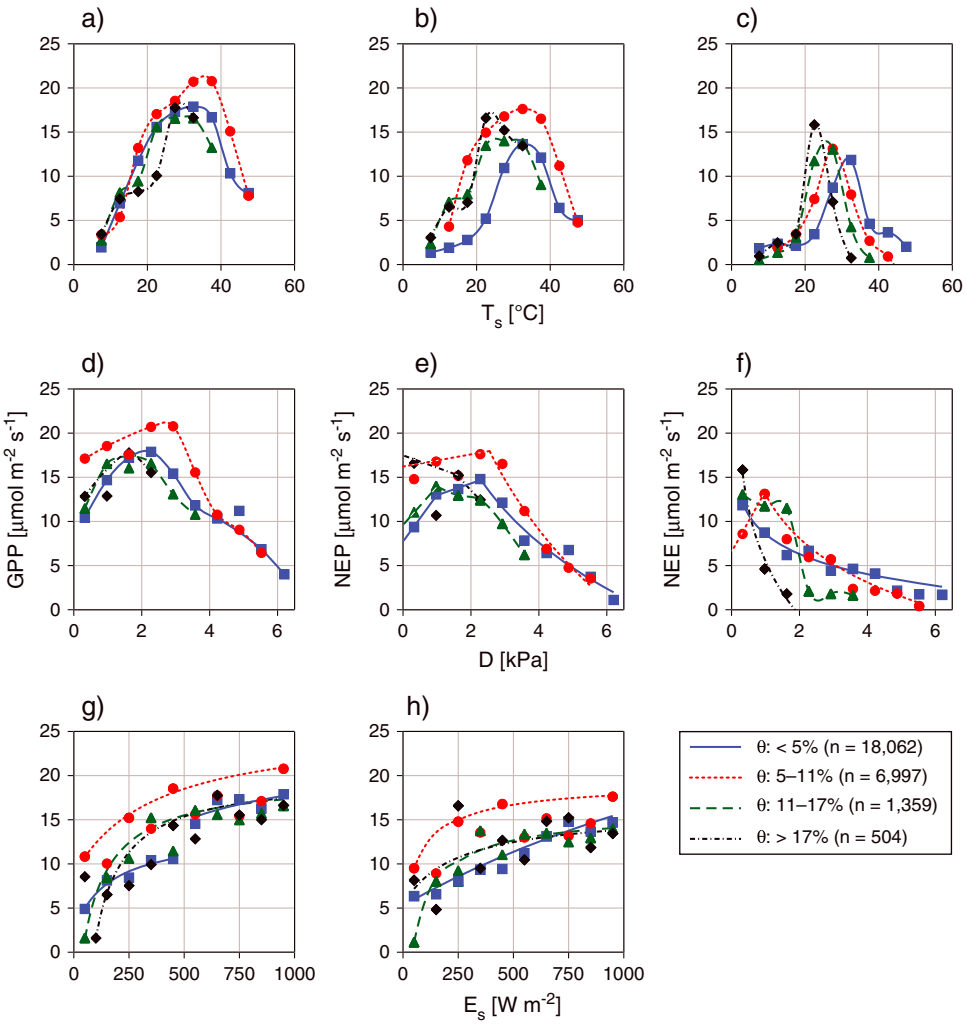

Figure 9. Parameter envelopes for GPP, NEP, and NEE as functions of 30 min θ and meteorological variables (T_s, D, or E_s). N = 26,922 30 min periods.

and 407 g C m^{-2} yr^{-1}, respectively; Table 2). During the first year, GPP was twice as large as in the following year (794 g C m^{-2} yr^{-1} and 398 g C m^{-2} yr^{-1}, respectively; Table 2).

[46] Peak GPP was 465 mmol m^{-2} day^{-1} (5.6 g C m^{-2} day^{-1}) in the first year (Sep 2010 to Aug 2011, n = 360 days) and 240 mmol m^{-2} day^{-1} (2.9 g C m^{-2} day^{-1}) second year (Sep 2011 to Aug 2012, n = 347 days; Figure 7). Average daily GPP was 184.0 ± 5.7 mmol m^{-2} day^{-1} (2.2 ± 0.07 g C m^{-2} day^{-1}) in the first year and 95.7 ± 2.4 mmol m^{-2} day^{-1} (1.1 ± 0.03 g C m^{-2} day^{-1}) in the second year. On average, GPP exceeded R_e by 49% in the first year, while GPP and R_e were closely matched in the second year (Table 2 and Figure 7). Seasonally, GPP and R_e were largest during the wet summer (DJF 2010–2011) and smallest in the following periods: during the dry summer (2011–2012), in November regardless of precipitation regime, and during both winters (JJA; Figure 7). Periods when GPP was consistently lower than R_e (i.e., GPP / R_e < 1) occurred in November 2010 and spring (SON) and summer 2011–2012 (Figure 7). Spikes of R_e occurred 1–2 days after the start of a precipitation event throughout the 2 year period of the study, with one exception in June 2011 when R_e did not increase in response to rainfall (Figure 7). GPP tended to be minimal during rainy periods and often but not always followed 2–5 days later by a large increase (Figure 7). Pulses in GPP were more frequent during the summer (DJF) and autumn (MAM) than in other seasons; for example, there was negligible increase in GPP in response to the first large rain in late October 2011 (Figure 7).

3.4. Ecosystem and Meteorological Drivers of GPP and R_e

[47] The envelope functions describing meteorological limits on daily-integrated GPP and R_e are shown in Figure 8. Daily GPP increased with increasing T_s across the low to moderate range (12–22°C) for all classes of soil moisture (Figure 8a), while there were few differences in GPP across moisture classes in this temperature range. However across the moderate-to-high range (22–38°C), GPP of the lowest θ was consistently smaller than that in the three larger classes of θ. A peak in GPP occurred in the range 22–28°C for the three largest classes of θ, but this was absent for the lowest class of θ (Figure 8a).

[48] A similar qualitative pattern in GPP as a function of D across the four classes of θ was apparent (Figure 8c). Maximal GPP occurred at about 1.5 kPa for the three largest

Table 3. Summary of Coherence Statistics[a]

	Period (Days)	|r|
	Summer (30 Dec 2010 to 3 Mar 2011)	
GPP-E_s	2.5–2.7	0.92
	6.4–8.0	0.96
GPP-T_s^{max}	2.5–2.7	0.94
R_e-E_s	6.4–8.0	0.93
	Winter (20 Jun to 22 Aug 2011)	
GPP-E_s	10.7	0.96
R_e-E_s	2.3	0.93
	10.7	0.97
R_e-T_s^{max}	4.0	0.96
	10.7	0.93
	Summer (30 Dec 2011 to 2 Mar 2012)	
GPP-T_s^{min}	2.9	0.98
GPP-D^{max}	2.9–3.2	0.96
GPP-D^{min}	2.9	0.92
GPP-P	5.3	0.93
R_e-E_s	2.4	0.96

[a]Period: 1/frequency [Hz]; |r|: magnitude of the correlation coefficient, calculated as the square root of the coherence in a given frequency range.

classes of θ and there was little difference in the response across these three classes of θ across the entire range of D. In contrast, GPP was essentially independent of D across the entire range for the smallest class of θ. As E_s increased from very low to high values (2–25 MJ m^{-2} d^{-1}), GPP increased with little difference in response between the three largest classes of θ (Figure 8e). Reductions in GPP at the largest values of E_s (> 22 MJ m^{-2} d^{-1}) were apparent in these three θ classes. For the lowest θ class, GPP was consistently smaller than in the other three classes when $E_s > 18$ MJ m^{-2} d^{-1}.

[49] Daily R_e increased with increasing T_s in all classes of θ. However, small reductions in R_e were observed at the largest values of T_s in the two intermediate classes of θ. In the smallest class of θ (< 4%), R_e did not show a decline at high values of T_s and was consistently smaller than that of the other three classes when $36°C > T_s > 22°C$ (Figure 8b). Daily ecosystem respiration was maximal at intermediate values of D (1–2 kPa) but declined at smaller or larger values of D for the three largest classes of θ (Figure 8d). In contrast, R_e increased approximately linearly with increasing D for the lowest class of θ (Figure 8d). Daily R_e increased with increasing E_s for low to moderate values of E_s in the three largest classes of θ but declined at the highest values of E_s (Figure 8f). In contrast in the smallest class of θ, R_e increased approximately linearly with increasing E_s (Figure 8f).

[50] As T_s increased, 30 min averaged values of GPP, NEP, and NEE increased to a peak value at moderate values of T_s but then declined with further increases in T_s across all four classes of θ (Figures 9a–9c). Temperature optima for GPP and NEP were in the range of approximately 30–38°C. The highest values of NEE fell into a narrow range of T_s (Figure 9c): 20–25°C (during the morning transition to turbulent conditions), 25–30°C (during nocturnal intermittent turbulence), 30–35°C (near-dusk turbulence events following calm conditions and little preceding photosynthesis). Maximal, 30 min averaged values of GPP and NEP were observed at moderate values of D (2–3 kPa), with smaller GPP and NEP observed at smaller or larger values of D (Figures 9d–f). GPP and NEP were larger for the intermediate class of θ (5–11%) for all except the largest D. In contrast, NEE tended to decrease with increasing D across the full range of D and in all classes of θ (Figure 9f). Thirty minute averaged values of GPP and NEP increased curvi-linearly with increasing E_s (Figures 9g and 9h). Both GPP and NEP approached an asymptotic value at full sunlight, except for the response of NEP in the smallest θ class, which did not approach an asymptotic value (Figure 9h).

[51] Storm conditions (low E_s, T_s, and D and high θ) typically persisted for 2–5 days, on average, while interstorm cycles were 5–11 days long (Table 3). During the wet summer (2010–2011), GPP was limited by reduced E_s and T_s^{max} during the storm, but during the interstorm interval, GPP and R_e responded positively only to increasing E_s (Table 3). Storms were less frequent in the winter; thus, interstorm intervals were longer (10.7 days) (Table 3). R_e responded to storm and interstorm fluctuations in E_s and T_s^{max} during the winter (Table 3). GPP responded to cycles of cloudiness rather than rainfall in the dry summer (2011–2012), while R_e responded only to fluctuations in E_s (Table 3).

4. Discussion

[52] Both gross primary production (GPP) and ecosystem respiration (R_e) were enhanced by the magnitude and frequency of storms, particularly during the extremely wet year (section 4.1). As hypothesized, the enhanced soil moisture, reduced vapor pressure deficit (D), and large solar irradiance (E_s) during cycles of storms and interstorms contributed to enhanced GPP in the wet year (section 4.2). As predicted in our third hypothesis, ecosystem responses to meteorological extremes in central Australia were related to large, seasonal responses of C_4 vegetation during summertime, creating a large carbon sink in the wet year (section 4.3). However, the dry year did not produce the large carbon source that is observed in other semi-arid regions where more decomposable substrate tends to accumulate (section 4.1). Ecosystem fluxes were coupled as hypothesized to photosynthesis of the C_3 Mulga canopy during dry periods, through which carbon neutrality (i.e., GPP:$R_e \approx 1$) was maintained by positive photosynthesis in low light and during the autumn after deep soil moisture had peaked (sections 4.2).

4.1. Large-Scale Patterns of Gross Primary Production, Ecosystem Respiration, and Carbon Budgets

[53] Average annual GPP at our site was large (50 mol m^{-2} yr^{-1}, 601 g C m^{-2} yr^{-1}) for a semi-arid ecosystem [cf. *Prentice et al*., 2001]. Relative to global biomes, carbon uptake in this study was larger than the annual average GPP in semi-arid or arid areas (19 mol m^{-2} yr^{-1}, 228 g C m^{-2} yr^{-1}) or tundra (24 mol m^{-2} yr^{-1}, 264 g C m^{-2} yr^{-1}); was about the same as the GPP of temperate grasslands and shrublands (40 mol m^{-2} yr^{-1}, 480 g C m^{-2} yr^{-1}) and boreal forests (50 mol m^{-2} yr^{-1}, 601 g C m^{-2} yr^{-1}); and was smaller than the GPP of temperate forests (79 mol m^{-2} yr^{-1}, 949 g C m^{-2} yr^{-1}), tropical savannas and grasslands (95 mol m^{-2} yr^{-1}, 1.14 kg C m^{-2} yr^{-1}), and tropical rainforests (193 mol m^{-2} yr^{-1}, 2.32 kg C m^{-2} yr^{-1}) [*Prentice et al*., 2001; *Beer et al*., 2010]. Intermediate in GPP between semi-arid and tropical savanna ecosystems, carbon uptake in this study was in general agreement with, although slightly larger than, GPP of a semi-arid C_4 grass and *Eucalyptus* savanna in Queensland Australia (32 mol m^{-2} yr^{-1}, 384 g C m^{-2} yr^{-1}) [*Hutley et al*., 2005]

but was substantially smaller than a tropical C_4 grass and *Eucalyptus* savanna in northern Australia (113–173 mol m^{-2} yr^{-1}, 1.36–2.08 kg C m^{-2} yr^{-1}) [*Chen et al*., 2003; *Hutley et al*., 2005; *Kanniah et al*., 2011]. The large annual GPP in this study (relative to other semi-arid regions) was the result of significant photosynthetic responses by the largely C_4 understorey to regular cycles of widespread, intense, and multiday storms (cf. Figures 6 and 7).

[54] Total annual GPP was larger in the wet year than in the dry year (Table 2). Reduction in productivity during dry periods has been extensively documented in annual- and continental-scale droughts in Europe, Australia, and the US [*Campos et al*., 2013], as well as in semi-arid shrublands in western North America [*Baldocchi*, 2008; *Scott et al*., 2009] where it is common for the carbon balance to switch from a sink to a source in response to drought [*Luo et al*., 2007; *Bowling et al*., 2010]. In the present study, a positive carbon balance was maintained during dry periods because reductions in GPP were compensated by proportional reductions in R_e (Figure 7). In addition, availability of θ or groundwater at depth contributes to maintenance of a carbon sink during the dry season in tropical north Australian savannas [*Hutley et al*., 2005; *Whitley et al*., 2011], in the first year of drought in the boreal zone of Canada [*Baldocchi*, 2008], and in tropical and humid forests [*Saleska et al*., 2003].

[55] Annual R_e was neither small nor large during the wet year but was small in the dry year (Table 2). In other semi-arid ecosystems having a similar mean annual temperature (25.0°C in this study), estimates of R_e range between 29 and 63 mol m^{-2} yr^{-1} (348–757 g C m^{-2} yr^{-1}) [*Bahn et al*., 2010], which is similar to, but generally larger than, R_e in the present study. There are two explanations for the small rates of R_e that were observed during the dry year: (1) θ was reduced, which inhibits heterotrophic respiration (R_h) [*Baldocchi*, 2008; *Bowling et al*., 2010; *Yan et al*., 2011; *Cable et al*., 2012], and (2) GPP was smaller in the dry year, with consequential reductions in substrate supply and hence autotrophic respiration (R_a) [*Janssens et al*., 2001; *Migliavacca et al*., 2011]. In the soils at our study site that are poor in organic matter: (a) R_h was small, (b) R_a was the dominant component of R_e, (c) the "basal" respiration rate (i.e., the decomposition rate of soil organic matter [*Kuzyakov and Gavrichkova*, 2010]) was negligible, and (d) reduction of substrate supply during the dry year contributed to maintaining a positive or neutral carbon budget (i.e., $GPP \geq R_e$), in contrast to grass-dominated savannas in semi-arid regions, which are a source of carbon during drought [*Scott et al*., 2009].

4.2. Daily to Seasonal Patterns of Production and Respiration

[56] Seasonally, GPP was smallest in the winter (JJA), largest in summer (DJF) and autumn (MAM), and mostly constrained to pulses following precipitation during the dry summer and autumn (Figure 7). Generally in semi-arid regions, the presence of a GPP response to a rainfall pulse is infrequently achieved because of the high frequency of very small (< 5 mm) events and unpredictability in the timing of large events [*Huxman et al*., 2004b; *Schwinning and Sala*, 2004; *Baldocchi*, 2008]. Summer rainfall in central and northern Australia, in contrast, occurs as large, multiday storm cycles (Figure 6) that are created by cyclic weakening of the monsoon depression [*Berry et al*., 2011]. This combination of soil moisture recharge following large storms and intervening periods of abundant sunlight acts to enhance GPP in central Australia.

[57] In the summer, pulses of GPP were synchronized with increasing leaf area index (LAI) of the understorey (Figure 7). Growth and assimilation in C_4 grasses are more likely to respond rapidly to rainfall than in C_3 woody vegetation when T_s and D are high [*Huxman et al*., 2004b; *Barron-Gafford et al*., 2007]. In contrast, Mulga is tolerant of low xylem water potentials (< −7 MPa) [*O'Grady et al*., 2009], which allows for small but continued physiological function at very low θ. After the sharp decline in T_s and D that occurred in February of each year (Figure 6), pulses of GPP were sustained longer and extended through the autumn across a month without substantial rainfall (Figure 7), thus reflecting continued use of soil water that is stored above the hardpan. C_3 woody vegetation can be active across a wide range of temperatures as a consequence of access to groundwater or θ reserves within the root zone [*Hastings et al*., 2005; *Baldocchi*, 2008; *Barron-Gafford et al*., 2012]. Likewise in this study, the magnitude of GPP pulses following summer rainfall depended upon (1) C_4 understorey growth in response to antecedent rainfall events and (2) Mulga production when it was not limited by high summer temperature or reduced θ.

[58] Like GPP, R_e was small in the winter, larger in the summer and autumn, and generally restricted to brief pulses in the dry year (Figure 7). Thermal sensitivity (i.e., the slope of the T_s-R_e^{night} curve, Q_{10}) was highest in the autumn and winter following the wet summer (curve 1, Figure 2), indicative of a larger decomposable substrate supply [*Lloyd and Taylor*, 1994; *Janssens et al*., 2001]. Substrate supply was large following senescence of the summer-active understorey and remained high through most of the following winter when microbial R_h was limited by low T_s and low θ (cf. Figures 2, 6, and 7). In contrast to other semi-arid regions where decomposable substrate accumulates under C_3 shrubs and trees that are typically deciduous [*Cable et al*., 2012], the majority of Australian woody vegetation is evergreen with sclerophyllous leaves that decompose slowly and contribute less to the availability of decomposable substrate than the episodic understorey with its large seasonal fluctuations in LAI and root turnover.

[59] Although R_e tended to be larger in the summer, R_e declined with very high temperature (Figures 3 and 8). Two explanations have been proposed for the apparent reduction of R_e at high temperatures in semi-arid ecosystems [*Anderson-Teixeira et al*., 2011]: (1) reduced substrate is available during dry or drought conditions due to reduced GPP at high temperature and (2) inverse autocorrelation exists between high temperature and soil moisture such that microbial respiration is limited by low θ during periods of high temperature. Reduction of R_e at high temperatures (i.e., thermal optimisation) in this study was the likely result of moisture restrictions on microbial decomposition, and that restriction occurred at a higher temperature in full sunlight than near dawn or dusk.

[60] In semi-arid regions, photodegradation is the physical means by which plant litter is degraded in full light, at high T_s, and in the absence of θ [*Gallo et al*., 2009; *Rutledge et al*., 2010]. Wintertime T_s^{max} was high enough to promote photodegradation of a substantial fraction of the

undecomposed litter, which was observed by the temporal correlation of wintertime R_e to T_s^{max} (Table 3). Photodegradation does not lead to full decomposition, and the remaining "photodegraded" litter can be a labile source of carbon [*Ma et al*., 2012], contributing to observed R_e responses to the early storms of spring and summer (Figure 7) in combination with flushing of CO_2 from soil pores through infiltration immediately following the first storm of the wet season (cf. Figure 7 and *Huxman et al*. [2004b]). Thus, during periods when GPP and R_a were small, R_h was responsive to microbial decomposition of the senescent understorey, photodegradation on warm days in the winter, displacement of CO_2 from soil pore spaces, and decomposition of photodegraded substrate following each of the first two large, springtime storms (Figure 7).

4.3. Subdaily Net Photosynthesis, Photosynthetic Light Responses, and Leaf Area Index

[61] Over subdaily time periods, GPP and NEP were limited by high and low values of T_s (> 40°C and < 20°C, respectively), large D (> 4 kPa), and low E_s (< 100 W m^{-2}; Figure 9). Low θ (< 5%) limited NEP at low to moderately high values of T_s (< 35°C; Figure 9) and wetter soil (5–10%) was associated with enhanced GPP and NEP (Figure 9). Apparent increases in GPP with increasing but low values of D reflected the autocorrelation of D and T_s in the early daylight hours. Thus, increasing D in the morning is caused by increased T_s, and this resulted in an apparent increase in GPP with increasing D (Figures 9a and 9d). Interestingly, the responses of GPP to D resembles the three-phase response of transpiration to increasing D [*Eamus and Shanahan*, 2002]: namely, increasing GPP at low values of D (Figures 9a and 9d), reaching a plateau or peak at low-to-moderate values of D, and finally declining with high D due to stomatal limitations, which suggests that it is likely that some features of the responses of GPP to D are attributable to stomatal function. Limitations on GPP and NEP due to low θ, high and low T_s, low E_s, and high D were autocorrelated over the course of a day and illustrative of the effects of meteorology on plant and ecosystem photosynthesis in this Mulga savanna (cf. Figures 6 and 9).

[62] When understorey LAI was small (< 0.5), NEP declined after midmorning, which lead to positive respiratory fluxes (i.e., NEE > 0 μmol m^{-2} s^{-1}) at midday in the spring (cf. Figures 4 and 7). *Scott et al*. [2010] observed moderate levels of positive net ecosystem respiration (i.e., NEE = 0–5 μmol m^{-2} s^{-1}) in full sunlight while the soil dried, comparable to NEE^{max} observed in this study (Figure 3). Midday depression of NEP in water-limited ecosystems is the result of three factors, singly or in combination [*Fu et al*., 2006]: (1) photoinhibition in chloroplasts and consequentially elevated R_a, (2) reduced stomatal opening in response to high D and low θ, or (3) increased R_h in the midday and afternoon heat. Midday depression of NEP during periods of low understorey LAI and following drought (cf. Figures 4 and 7) was offset by positive assimilation rates in the morning by Mulga (cf. Figure 4 and Table 1) and possibly by photosynthesis in the cryptobiotic soil crust [*Jameson*, 2012].

[63] Photosynthetic responses to light were largest when LAI of the canopy and understorey was high (total LAI > 0.5; Figure 7). When understorey LAI was high, NEP did not saturate in full sunlight (Figure 5c), which is a characteristic of C_4 vegetation [*Hattersley*, 1983]. Conversely, photosynthesis in Mulga, which are relicts of former central Australian rainforest understorey vegetation [*Martin*, 2006], saturated at moderate light levels (i.e., a large quantum yield, α; Table 1). The combination of these photosynthetic responses resulted in ecosystem LRFs that were characterized by large quantum yield (i.e., the initial slope of the LRF, α), large NEP^{max}, and failure to reach photosynthetic saturation in full sunlight (Figure 5c). Because of these photosynthetic characteristics of Mulga and C_4 grasses, Mulga savannas of central Australia have the potential to generate large, positive carbon budgets (i.e., $GPP > R_e$) across vast areas of the Australian continent, particularly following infrequent rainfall events.

5. Conclusions

[64] Among semi-arid and arid regions of the world, the tropical Mulga savannas of central and northern Australia are distinguished by large gross primary production (GPP) and low-to-moderate rates of ecosystem respiration (R_e). Over the 2 years of this study, the amount of rainfall was more than 250 mm above the long-term average in the first year and more than 100 mm below the long-term average in the second year. Across these 2 years, the carbon budget shifted from a strong carbon sink to carbon neutral (i.e., $GPP = R_e$). Three main conclusions were drawn from this study:

[65] 1. Ecosystem photosynthesis was enhanced by extreme and cyclic rainfall events that occur across northern and central Australia. Even during one of these wet (much higher than average rainfall) years, the monsoon depression experiences cyclic weakening that leads to interstorm periods of large solar irradiance (E_s), high soil temperature (T_s), and high vapor pressure deficit (D). It is the abundant light and soil moisture that characterizes these interstorm periods and stimulates growth and photosynthesis in the C_4 understorey (cf. Tables 1 and 3, Figure 7). In contrast, Mulga photosynthesis was stimulated when moisture stores below 1 m were recharged (cf. Figures 6 and 7) and when neither high T_s nor D limited photosynthesis (cf. Table 3, Figures 6 and 7).

[66] 2. Spatial heterogeneity of soil hardpan at depth and resultant soil moisture (θ) provides storage reservoirs at various depths, facilitating photosynthesis by both deep- and shallow-rooted species. Recharge events like the first year are uncommon, and decades may pass between the largest storm seasons [*Ganter and Tobin*, 2012]. In contrast to semi-arid areas with limited recharge below 50 cm [*Kurc and Small*, 2007], θ was recharged regularly in the dry year (Figure 6) because of the large infiltration rates in kandosol soil. Mulga has survived through Australia's drying climate over the past 0.5 Myr [*Martin*, 2006] in the face of an indeterminately long wait for the return of favorable conditions through (a) tolerance of low xylem water potential and (b) efficient and nearly exclusive use of stored soil water. The small but positive morning photosynthesis in Mulga, which is supported by storage of θ in shallow soil depths (in the top several meters), contributes to maintenance of a neutral carbon balance during moisture-limited periods.

[67] 3. The two largest sources of R_e in this study were autotrophic respiration (R_a) by the seasonal understorey and heterotrophic respiration (R_h) by decomposition of fresh or "photodegraded" organic matter (i.e., priming) following understorey senescence. The pattern of R_e followed closely

that of understorey LAI and R_a, except in March 2011 when R_e was larger than R_a and thereby indicative of large R_h due to the decomposition of senescent vegetation. In general, R_e was limited by availability of decomposable biomass (i.e., substrate limitation), θ (i.e., moisture limitation), and temperature (i.e., thermal sensitivity), although these factors varied in synchrony with storm cycles so that no single factor explained variations in R_e.

[68] The close association between GPP, R_e, and precipitation pulses in central Australia suggests that large areas of Australia may be more of a carbon sink, and a smaller carbon source, than previously expected. Rainfall caused corresponding pulses of GPP and R_e. These pulses were distinguished in wet and dry years by their size and the relative proportion of canopy and understorey LAI that contributed to the response. All primary producer types (trees, seasonal grasses and shrubs, and cryptobiotic crust) contributed to maintaining the carbon balance in drought conditions and across seasons.

[69] **Acknowledgments.** This work was supported by grants from the Australian Government's Terrestrial Ecosystems Research Network (TERN) (www.tern.gov.au) and the National Centre for Groundwater Research and Training (NCGRT, an Australian Government initiative supported by the Australian Research Council and the National Water Commission). This work was supported also by OzFlux and the Australian Supersite Network, both parts of TERN and the latter of which is a research infrastructure facility established under the National Collaborative Research Infrastructure Strategy and Education Infrastructure Fund, Super Science Initiative, through the Department of Industry, Innovation, Science, Research, and Tertiary Education. We would like to thank Peter Isaac for his assistance with data analysis. We would also like to thank A. O'Grady and an anonymous reviewer for their assistance in improving this manuscript.

References

Abramowitz, G., H. Gupta, A. Pitman, Y. Wang, R. Leuning, H. Cleugh, and K. L. Hsu (2006), Neural Error Regression Diagnosis (NERD): A tool for model bias identification and prognostic data assimilation, *J. Hydrol.*, *7*, 160–177.

American Meteorological Society (AMS) (1997), Meteorological drought, *Bull. Am. Meteorol. Soc.*, *78*, 847–849.

Anderson-Teixeira, K. J., J. P. Delong, A. M. Fox, D. A. Brese, and M. E. Litvak (2011), Differential responses of production and respiration to temperature and moisture drive the carbon balance across a climatic gradient in New Mexico, *Glob. Change Biol.*, *17*, 410–424, doi:10.1111/j.1365-2486.2010.02269.x.

Atkin, O. K., J. R. Evans, and K. Siebke (1998), Relationship between the inhibition of leaf respiration by light and enhancement of leaf dark respiration following light treatment, *Aust. J. Plant Physiol.*, *25*, 437–443, doi:10.1071/PP97159.

Aubinet, M. (2008), Eddy covariance CO_2 flux measurements in nocturnal conditions: An analysis of the problem, *Ecol. Appl.*, *18*, 1368–1378.

Bahn, M., et al. (2010), Soil respiration at mean annual temperature predicts annual total across vegetation types and biomes, *Biogeosciences*, *7*, 2147–2157, doi:10.5194/bg-7-2147-2010.

Baldocchi, D. (2008), Breathing of the terrestrial biosphere: lessons learned from a global network of carbon dioxide flux measurement systems, *Aust. J. Bot.*, *56*, 1–26, doi:10.1071/BT07151.

Barbour, M. M., N. G. McDowell, G. Tcherkez, C. P. Bickford, and D. T. Hanson (2007), A new measurement technique reveals rapid post-illumination changes in the carbon isotope composition of leaf-respired CO_2, *Plant Cell Environ.*, *30*, 469–482, doi:10.1111/j.1365-3040.2007.01634.x.

Barbour, M. M., J. E. Hunt, N. Kodama, J. Laubach, T. M. McSeveny, G. N. D. Rogers, G. Tcherkez, and L. Wingate (2011), Rapid changes in delta 13^C of ecosystem-respired CO_2 after sunset are consistent with transient 13^C enrichment of leaf respired CO_2, *New Phytol.*, *190*, 990–1002, doi:10.1111/j.1469-8137.2010.03635.x.

Barron-Gafford, G. A., K. A. Grieve, and R. Murthy (2007), Leaf- and stand-level responses of a forested mesocosm to independent manipulations of temperature and vapor pressure deficit, *New Phytol.*, *174*, 614–625, doi:10.1111/j.1469-8137.2007.02035.x.

Barron-Gafford, G. A., R. L. Scott, G. D. Jenerette, E. P. Hamerlynck, and T. E. Huxman (2012), Temperature and precipitation controls over leaf- and ecosystem-level CO_2 flux along a woody plant encroachment gradient, *Glob. Change Biol.*, *18*, 1389–1400, doi:10.1111/j.1365-2486.2011.02599.x.

Beer, C., et al. (2010), Terrestrial gross carbon dioxide uptake: Global distribution and covariation with climate, *Science*, *329*, 834–838, doi:10.1126/science.1184984.

Berry, G., M. J. Reeder, and C. Jakob (2011), Physical mechanisms regulating summertime rainfall over northwestern Australia, *J. Clim.*, *24*, 3705–3717, doi:10.1175/2011jcli3943.1.

Bowling, D. R., S. Bethers-Marchetti, C. K. Lunch, E. E. Grote, and J. Belnap (2010), Carbon, water, and energy fluxes in a semiarid cold desert grassland during and following multiyear drought, *J. Geophys. Res.*, *115*, G04026, doi:10.1029/2010JG001322.

Bowman, D., et al. (2010), Biogeography of the Australian monsoon tropics, *J. Biogeogr.*, *37*, 201–216, doi:10.1111/j.1365-2699.2009.02210.x.

Cable, J. M., G. A. Barron-Gafford, K. Ogle, M. Pavao-Zuckerman, R. L. Scott, D. G. Williams, and T. E. Huxman (2012), Shrub encroachment alters sensitivity of soil respiration to temperature and moisture, *J. Geophys. Res.*, *117*, G01001, doi: 10.1029/2011jg001757.

Campbell Scientific Inc. (2004), Open path eddy covariance system operator's manual, edited, Logan, UT, USA.

Campos, G. E. P., et al. (2013), Ecosystem resilience despite large–scale altered hydroclimate conditions, *Nature*, *494*, 349–352, doi:10.1038/nature11836.

Chen, X. Y., J. M. Bowler, and J. W. Magee (1991), Aeolian landscapes in central Australia - gypsiferous and quartz dune environments from Lake Amadeus, *Sedimentology*, *38*, 519–538.

Chen, X. Y., L. B. Hutley, and D. Eamus (2003), Carbon balance of a tropical savanna of northern Australia, *Oecologia*, *137*, 405–416, doi:10.1007/s00442-003-1358-5.

Christie, E. K. (1975), Physiological responses of semiarid grasses. IV* Photosynthetic rates of *Thyridolepis mitchelliana* and *Cenchrus ciliaris* leaves, *Aust. J. Agric. Res.*, *26*, 459–466, doi:10.1071/ar9750459.

Cleverly, J. (2011), Alice Springs Mulga OzFlux site, OzFlux: Australian and New Zealand Flux Research and Monitoring Network, hdl: 102.100.100/8697.

Cleverly, J. R., C. N. Dahm, J. R. Thibault, D. J. Gilroy, and J. E. A. Coonrod (2002), Seasonal estimates of actual evapo-transpiration from *Tamarix ramosissima* stands using three-dimensional eddy covariance, *J. Arid Environ.*, *52*, 181–197, doi:10.1006/jare.2002.0972.

Coles, S. (2001), *An introduction to statistical modeling of extreme values*, Springer Verlag, London, UK, pp. 208.

Dai, A. (2011), Drought under global warming: a review, *Clim. Change*, *2*, 45–65, doi:10.1002/wcc.81.

Eamus, D. (2003), How does ecosystem water balance affect net primary productivity of woody ecosystems?, *Funct. Plant Biol.*, *30*, 187–205, doi:10.1071/FP02084.

Eamus, D., and L. Prior (2001), Ecophysiology of trees of seasonally dry tropics: Comparisons among phenologies, in *Advances in Ecological Research*, Academic Press Ltd, London, vol. *32*, pp. 113–197.

Eamus, D., and S. T. Shanahan (2002), A rate equation model of stomatal responses to vapour pressure deficit and drought, *BMC Ecology*, *2*, 8.

Eamus, D., T. Hatton, P. Cook, and C. Colvin (2006), *Ecohydrology. Vegetation function, water and resource management*, CSIRO Publishing, Collingwood, VIC, pp. 348.

Eamus, D., J. Cleverly, N. Boulain, N. Grant, R. Faux, and R. Villalobos-Vega (2013), Carbon and water fluxes in an arid-zone *Acacia* savanna woodland: An analyses of seasonal patterns and responses to rainfall events, *Agric. For. Meteor.*, doi:10.1016/j.agrformet.2013.04.020.

Fu, Y. L., G. R. Yu, X. M. Sun, Y. N. Li, X. F. Wen, L. M. Zhang, Z. Q. Li, L. Zhao, and Y. B. Hao (2006), Depression of net ecosystem CO_2 exchange in semi-arid *Leymus chinensis* steppe and alpine shrub, *Agric. For. Meteor.*, *137*, 234–244, doi:10.1016/j.agrformet.2006.02.009.

Gallo, M. E., A. Porras-Alfaro, K. J. Odenbach, and R. L. Sinsabaugh (2009), Photoacceleration of plant litter decomposition in an arid environment, *Soil Biol. Biochem.*, *41*, 1433–1441, doi:10.1016/j.soilbio.2009.03.025.

Ganter, C., and S. Tobin (2012), [Regional Climates] Australia [in "State of the Climate in 2011"], *Bull. Am. Meteorol. Soc.*, *93*, S218–S221.

Hastings, S. J., W. C. Oechel, and A. Muhlia-Melo (2005), Diurnal, seasonal and annual variation in the net ecosystem CO_2 exchange of a desert shrub community (Sarcocaulescent) in Baja California, Mexico, *Glob. Change Biol.*, *11*, 927–939, doi:10.1111/j.1365-2486.2005.00951.x.

Hattersley, P. W. (1983), The distribution of C_3 and C_4 grasses in Australia in relation to climate, *Oecologia*, *57*, 113–128, doi:10.1007/bf00379569.

Hsu, K.-l., H. V. Gupta, X. Gao, S. Sorooshian, and B. Imam (2002), Self-organizing linear output map (SOLO): An artificial neural network suitable for hydrologic modeling and analysis, *Water Resour. Res.*, *38*, 1302, doi:10.1029/2001wr000795.

Hutley, L. B., R. Leuning, J. Beringer, and H. A. Cleugh (2005), The utility of the eddy covariance techniques as a tool in carbon accounting: tropical savanna as a case study, *Aust. J. Bot.*, *53*, 663–675, doi:10.1071/BT04147.

Hutley, L. B., J. Beringer, P. R. Isaac, J. M. Hacker, and L. A. Cernusak (2011), A sub-continental scale living laboratory: Spatial patterns of savanna vegetation over a rainfall gradient in northern Australia, *Agric. For. Meteor.*, *151*, 1417–1428, doi:10.1016/j.agrformet.2011.03.002.

Huxman, T. E., J. M. Cable, D. D. Ignace, J. A. Eilts, N. B. English, J. Weltzin, and D. G. Williams (2004a), Response of net ecosystem gas exchange to a simulated precipitation pulse in a semi-arid grassland: the role of native versus non-native grasses and soil texture, *Oecologia*, *141*, 295–305, doi:10.1007/s00442-003-1389-y.

Huxman, T. E., K. A. Snyder, D. Tissue, A. J. Leffler, K. Ogle, W. T. Pockman, D. R. Sandquist, D. L. Potts, and S. Schwinning (2004b), Precipitation pulses and carbon fluxes in semiarid and arid ecosystems, *Oecologia*, *141*, 254–268, doi:10.1007/s00442-004-1682-4.

Jameson, J. (2012), The importance of biological soil crust in Australian semi-arid ecosystems, B.Sc. (Honours) thesis, University of Technology, Sydney, Sydney, NSW, Australia.

Janssens, I. A., et al. (2001), Productivity overshadows temperature in determining soil and ecosystem respiration across European forests, *Glob. Change Biol.*, *7*, 269–278, doi:10.1046/j.1365-2486.2001.00412.x.

Kanniah, K. D., J. Beringer, and L. B. Hutley (2011), Environmental controls on the spatial variability of savanna productivity in the Northern Territory, Australia, *Agric. For. Meteor.*, *151*, 1429–1439, doi:10.1016/j.agrformet.2011.06.009.

Kong, Q., and S. Zhao (2010), Heavy rainfall caused by interactions between monsoon depression and middle-latitude systems in Australia: a case study, *Meteorol. Atmos. Phys.*, *106*, 205–226, doi:10.1007/s00703-010-0060-5.

Kurc, S. A., and E. E. Small (2007), Soil moisture variations and ecosystem-scale fluxes of water and carbon in semiarid grassland and shrubland, *Water Resour. Res.*, *43*, W06416, doi:10.1029/2006wr005011.

Kuzyakov, Y., and O. Gavrichkova (2010), REVIEW: Time lag between photosynthesis and carbon dioxide efflux from soil: a review of mechanisms and controls, *Glob. Change Biol.*, *16*, 3386–3406, doi:10.1111/j.1365-2486.2010.02179.x.

Lasslop, G., M. Reichstein, D. Papale, A. D. Richardson, A. Arneth, A. Barr, P. Stoy, and G. Wohlfahrt (2010), Separation of net ecosystem exchange into assimilation and respiration using a light response curve approach: critical issues and global evaluation, *Glob. Change Biol.*, *16*, 187–208, doi:10.1111/j.1365-2486.2009.02041.x.

Lasslop, G., et al. (2012), On the choice of the driving temperature for eddy-covariance carbon dioxide flux partitioning, *Biogeosciences*, *9*, 5243–5259, doi:10.5194/bg-9-5243-2012.

Liu, R., Y. Li, and Q. X. Wang (2012), Variations in water and CO_2 fluxes over a saline desert in western China, *Hydrol. Process.*, *26*, 513–522, doi:10.1002/hyp.8147.

Lloyd, J., and J. A. Taylor (1994), On the temperature-dependence of soil respiration, *Funct. Ecol.*, *8*, 315–323.

Luo, H. Y., W. C. Oechel, S. J. Hastings, R. Zulueta, Y. H. Qian, and H. Kwon (2007), Mature semiarid chaparral ecosystems can be a significant sink for atmospheric carbon dioxide, *Glob. Change Biol.*, *13*, 386–396, doi:10.1111/j.1365-2486.2006.01299.x.

Ma, S., D. D. Baldocchi, J. A. Hatala, M. Detto, and J. Curiel-Yuste (2012), Are rain-induced ecosystem respiration pulses enhanced by legacies of antecedent photodegradation in semi-arid environments?, *Agric. For. Meteor.*, *154*, 203–213, doi:10.1016/j.agrformet.2011.11.007.

Macfarlane, C., M. Hoffman, D. Eamus, N. Kerp, S. Higginson, R. McMurtrie, and M. Adams (2007), Estimation of leaf area index in eucalypt forest using digital photography, *Agric. For. Meteor.*, *143*, 176–188, doi:10.1016/j.agrformet.2006.10.013.

Martin, H. A. (2006), Cenozoic climatic change and the development of the arid vegetation in Australia, *J. Arid Environ.*, *66*, 533–563, doi:10.1016/j.jaridenv.2006.01.009.

Massman, W., and R. Clement (2004), Uncertainty in eddy covariance flux estimates resulting from spectral attenuation, in *Handbook of Micrometeorology: A guide for Surface Flux Measurement and Analysis*, edited by X. Lee, W. Massman, and B. Law, Kluwer Academic Publishers, Dordrecht/Boston/London, pp. 67–100.

Migliavacca, M., et al. (2011), Semiempirical modeling of abiotic and biotic factors controlling ecosystem respiration across eddy covariance sites, *Glob. Change Biol.*, *17*, 390–409, doi:10.1111/j.1365-2486.2010.02243.x.

Mitchell, S., K. Beven, J. Freer, and B. Law (2011), Processes influencing model-data mismatch in drought-stressed, fire-disturbed eddy flux sites, *J. Geophys. Res.*, *116*, G02008, doi:10.1029/2009jg001146.

Morton, S. R., et al. (2011), A fresh framework for the ecology of arid Australia, *J. Arid Environ.*, *75*, 313–329, doi:10.1016/j.jaridenv.2010.11.001.

Nicholas, A. M. M., D. C. Franklin, and D. M. J. S. Bowman (2011), Floristic uniformity across abrupt boundaries between *Triodia* hummock grassland and *Acacia* shrubland on an Australian desert sandplain, *J. Arid Environ.*, *75*, 1090–1096, doi:10.1016/j.jaridenv.2011.06.016.

O'Grady, A. P., P. G. Cook, D. Eamus, A. Duguid, J. D. H. Wischusen, T. Fass, and D. Worldege (2009), Convergence of tree water use within an arid-zone woodland, *Oecologia*, *160*, 643–655, doi:10.1007/s00442-009-1332-y.

Oliveira, P. E. S., O. C. Acevedo, O. L. L. Moraes, H. R. Zimermann, and C. Teichrieb (2013), Nocturnal intermittent coupling between the interior of a pine forest and the air above it, *Bound.-Lay. Meteor.*, *146*, 45–64, doi:10.1007/s10546-012-9756-z.

Papalexiou, S. M., and D. Koutsoyiannis (2013), Battle of extreme value distributions: A global survey on extreme daily rainfall, *Water Resour. Res.*, *49*, 187–201, doi:10.1029/2012WR012557.

Prentice, I. C., et al. (2001), The carbon cycle and atmospheric carbon dioxide, in *Climate Change 2001: The Scientific Basis. Contribution of Working Group I to the Third Assessment Report on the Intergovernmental Panel on Climate Change*, edited by J. T. Houghton, Y. Ding, D. J. Griggs, M. Noguer, P. J. van der Linden, X. Dai, K. Maskell, and C. A. Johnson, pp. 183–237, Cambridge University Press, Cambridge.

Reichstein, M., et al. (2005), On the separation of net ecosystem exchange into assimilation and ecosystem respiration: review and improved algorithm, *Glob. Change Biol.*, *11*, 1424–1439, doi:10.1111/j.1365-2486.2005.001002.x.

Reynolds, J. F., R. A. Virginia, P. R. Kemp, A. G. de Soyza, and D. C. Tremmel (1999), Impact of drought on desert shrubs: Effects of seasonality and degree of resource island development, *Ecol. Monogr.*, *69*, 69–106.

Rutledge, S., D. I. Campbell, D. Baldocchi, and L. A. Schipper (2010), Photodegradation leads to increased carbon dioxide losses from terrestrial organic matter, *Glob. Change Biol.*, *16*, 3065–3074, doi:10.1111/j.1365-2486.2009.02149.x.

Saleska, S. R., et al. (2003), Carbon in amazon forests: Unexpected seasonal fluxes and disturbance-induced losses, *Science*, *302*, 1554–1557, doi:10.1126/science.1091165.

Schmidt, S., R. E. Lamble, R. J. Fensham, and I. Siddique (2010), Effect of woody vegetation clearing on nutrient and carbon relations of semi-arid dystrophic savanna, *Plant Soil*, *331*, 79–90, doi:10.1007/s11104-009-0233-5.

Schotanus, P., F. T. M. Nieuwstadt, and H. A. R. Debruin (1983), Temperature-measurement with a sonic anemometer and its application to heat and moisture fluxes, *Bound.-Lay. Meteor.*, *26*, 81–93.

Schwinning, S., and O. E. Sala (2004), Hierarchy of responses to resource pulses in arid and semi-arid ecosystems, *Oecologia*, *141*, 211–220, doi:10.1007/s00442-004-1520-8.

Scott, R. L., G. D. Jenerette, D. L. Potts, and T. E. Huxman (2009), Effects of seasonal drought on net carbon dioxide exchange from a woody-plant-encroached semiarid grassland, *J. Geophys. Res.*, *114*, G04004, doi:10.1029/2008jg000900.

Scott, R. L., E. P. Hamerlynck, G. D. Jenerette, M. S. Moran, and G. A. Barron-Gafford (2010), Carbon dioxide exchange in a semidesert grassland through drought-induced vegetation change, *J. Geophys. Res.*, *115*, G03026, doi:10.1029/2010jg001348.

Simon, B. K., and Y. Alfonso (2011), AusGrass2, http://ausgrass2.myspecies.info/, accessed 31 January 2013.

van Gorsel, E., R. Leuning, H. A. Cleugh, H. Keith, M. U. F. Kirschbaum, and T. Suni (2008), Application of an alternative method to derive reliable estimates of nighttime respiration from eddy covariance measurements in moderately complex topography, *Agric. For. Meteor.*, *148*, 1174–1180, doi:10.1016/j.agrformet.2008.01.015.

van Gorsel, E., et al. (2009), Estimating nocturnal ecosystem respiration from the vertical turbulent flux and change in storage of CO_2, *Agric. For. Meteor.*, *149*, 1919–1930, doi:10.1016/j.agrformet.2009.06.020.

van Gorsel, E., I. N. Harman, J. J. Finnigan, and R. Leuning (2011), Decoupling of air flow above and in plant canopies and gravity waves affect micrometeorological estimates of net scalar exchange, *Agric. For. Meteor.*, *151*, 927–933, doi:10.1016/j.agrformet.2011.02.012.

Van Etten, E. J. B. (2009), Inter-annual rainfall variability of arid Australia: Greater than elsewhere?, *Aust. Geogr.*, *40*, 109–120, doi:10.1080/00049180802657075.

Warner, T. T. (2004), *Desert Meteorology*, Cambridge University Press, Cambridge UK, pp. 595.

Webb, E., G. Pearman, and R. Leuning (1980), Correction of flux measurements for density effects due to heat and water-vapor transfer, *Q. J. Roy. Meteor. Soc.*, *106*, 85–100.

Wesely, M. L. (1970), Eddy correlation measurements in the atmospheric surface layer over agricultural crops, Ph.D. Dissertation thesis, 102 pp., University of Wisconsin, Madison.

Whitley, R., B. Medlyn, M. Zeppel, C. Macinnis-Ng, and D. Eamus (2009), Comparing the Penman-Monteith equation and a modified Jarvis-Stewart model with an artificial neural network to estimate stand-scale transpiration and canopy conductance, *J. Hydrol.*, *373*, 256–266, doi:10.1016/j.jhydrol.2009.04.036.

Whitley, R. J., C. M. O. Macinnis-Ng, L. B. Hutley, J. Beringer, M. Zeppel, M. Williams, D. Taylor, and D. Eamus (2011), Is productivity of mesic savannas light limited or water limited? Results of a simulation study, *Glob. Change Biol.*, *17*, 3130–3149, doi:10.1111/j.1365-2486.2011.02425.x.

Wohlfahrt, G., M. Bahn, A. Haslwanter, C. Newesely, and A. Cernusca (2005), Estimation of daytime ecosystem respiration to determine gross primary production of a mountain meadow, *Agric. For. Meteor.*, *130*, 13–25, doi:10.1016/j.agrformet.2005.02.001.

Wohlfahrt, G., L. F. Fenstermaker, and J. A. Arnone (2008), Large annual net ecosystem CO_2 uptake of a Mojave Desert ecosystem, *Glob. Change Biol.*, *14*, 1475–1487, doi:10.1111/j.1365-2486.2008.01593.x.

Yan, L. M., S. P. Chen, J. H. Huang, and G. H. Lin (2011), Water regulated effects of photosynthetic substrate supply on soil respiration in a semiarid steppe, *Glob. Change Biol.*, *17*, 1990–2001, doi:10.1111/j.1365-2486.2010.02365.x.

Zhang, H. Q. (2010), Diagnosing Australia-Asian monsoon onset/retreat using large-scale wind and moisture indices, *Clim. Dyn.*, *35*, 601–618, doi:10.1007/s00382-009-0620-x.